Versatile Coordination of Cyclopentadienyl-Arene Ligands and Its Role in Titanium-Catalyzed Ethylene Trimerization

Edwin Otten, Aurora A. Batinas, Auke Meetsma, and Bart Hessen*

Center for Catalytic Olefin Polymerization, Stratingh Institute for Chemistry, University of Groningen, Nijenborgh 4, 9747 AG, Groningen, The Netherlands

Received January 4, 2009; E-mail: b.hessen@rug.nl

Abstract: Cationic titanium(IV) complexes with *ansa*-(η^5-cyclopentadienyl,η^6-arene) ligands were synthesized and characterized by X-ray crystallography. The strength of the metal−arene interaction in these systems was studied by variable-temperature NMR spectroscopy. Complexes with a C_1 bridge between the cyclopentadienyl and arene moieties feature hemilabile coordination behavior of the ligand and consequently are active ethylene trimerization catalysts. Reaction of the titanium(IV) dimethyl cations with CO results in conversion to the analogous cationic titanium(II) dicarbonyl species. Metal-to-ligand backdonation in these formally low-valent complexes gives rise to a strongly bonded, partially reduced arene moiety. In contrast to the η^6-arene coordination mode observed for titanium, the more electron-rich vanadium(V) cations [cyclopentadienyl-arene]V(N^{i}Pr$_2$)(NC$_6$H$_4$-4-Me)$^+$ feature η^1-arene binding, as determined by a crystallographic study. The three different metal−arene coordination modes that we experimentally observed model intermediates in the cycle for titanium-catalyzed ethylene trimerization. The nature of the metal−arene interaction in these systems was studied by DFT calculations.

Introduction

Ancillary ligands play a pivotal role in catalysis by transition metal complexes by modulating the steric and electronic environment around the metal center. One particular class is formed by *hemilabile* ligands (i.e., ligands possessing a combination of tightly bound and substitutionally labile groups). These are of interest as they can (transiently) stabilize intermediate reactive species, while still allowing subsequent reactivity.[1,2] Most hemilabile ligands are multidentates that feature one pendant Lewis base moiety that is less strongly binding than the others, and that can readily and reversibly dissociate. Phosphine ligands that contain additional labile donors, such as O- or N-based functionalities, have received most attention.[3−7] Another prominent class of hemilabile ligands is formed by donor-functionalized cyclopentadienyl ligands, bearing pendant P, As, S,[8] or O groups[9] that interact weakly with the metal center; transition metal complexes of these are known across the periodic table. Arene-substituted phosphine ligands, in which the pendant arene functions as weakly

coordinating group are also known,[10−12] and studies on arene exchange (hemilability) in such compounds have been reported.[13−15] The combination of a monoanionic anchoring group with a pendant arene as labile moiety is less common, but aryloxide ligands that contain aromatic substituents on the 2,6-positions of the central phenoxide ring have been shown to coordinate to low-valent group 6 metals in a chelating (O,η^6-arene) mode.[16−19] A comprehensive review on the synthesis and properties of transition metal complexes of tethered arenes has recently appeared.[20]

Previously, we reported that cationic half-sandwich complexes of titanium are transformed from ethylene polymerization catalysts into selective ethylene *trimerization* catalysts (producing 1-hexene) when the cyclopentadienyl ligand bears a hemilabile pendant arene substituent.[21,22] Subsequently, titanium complexes with cyclopentadienyl ligands incorporating other

(1) Slone, C. S.; Weinberger, D. A.; Mirkin, C. A. *Prog. Inorg. Chem.* **1999**, *48*, 233.
(2) Braunstein, P.; Naud, F. *Angew. Chem., Int. Ed.* **2001**, *40*, 680.
(3) Jeffrey, J. C.; Rauchfuss, T. B. *Inorg. Chem.* **1979**, *18*, 2658.
(4) Grotjahn, D. B.; Gong, Y.; Zakharov, L.; Golen, J. A.; Rheingold, A. L. *J. Am. Chem. Soc.* **2006**, *128*, 438.
(5) Kuriyama, M.; Nagai, K.; Yamada, K.; Miwa, Y.; Taga, T.; Tomioka, K. *J. Am. Chem. Soc.* **2002**, *124*, 8932.
(6) Moxham, G. L.; Randell-Sly, H. E.; Brayshaw, S. K.; Woodward, R. L.; Weller, A. S.; Willis, M. C. *Angew. Chem., Int. Ed.* **2006**, *45*, 7618.
(7) Müller, C.; Lachicotte, R. J.; Jones, W. D. *Organometallics* **2002**, *21*, 1975.
(8) Butenschön, H. *Chem. Rev.* **2000**, *100*, 1527.
(9) Siemeling, U. *Chem. Rev.* **2000**, *100*, 1495.
(10) Singewald, E. T.; Mirkin, C. A.; Stern, C. L. *Angew. Chem., Int. Ed.* **1995**, *34*, 1624.
(11) Werner, H. *Dalton Trans.* **2003**, 3829.
(12) Montag, M.; Leitus, G.; Shimon, L. J. W.; Ben-David, Y.; Milstein, D. *Chem.-Eur. J.* **2007**, *13*, 9043.
(13) Singewald, E. T.; Mirkin, C. A.; Levy, A. D.; Stern, C. L. *Angew. Chem., Int. Ed.* **1994**, *33*, 2473.
(14) Singewald, E. T.; Shi, X.; Mirkin, C. A.; Schofer, S. J.; Stern, C. L. *Organometallics* **1996**, *15*, 3062.
(15) Traylor, T. G.; Goldberg, M. J. *Organometallics* **1987**, *6*, 2413.
(16) Kerschner, J. L.; Fanwick, P. E.; Rothwell, I. P. *J. Am. Chem. Soc.* **1987**, *109*, 5840.
(17) Kerschner, J. L.; Fanwick, P. E.; Rothwell, I. P. *J. Am. Chem. Soc.* **1988**, *110*, 8235.
(18) Lockwood, M. A.; Fanwick, P. E.; Rothwell, I. P. *Polyhedron* **1995**, *14*, 3363.
(19) Lentz, M. R.; Fanwick, P. E.; Rothwell, I. P. *Organometallics* **2003**, *22*, 2259.
(20) Adams, J. R.; Bennett, M. A. *Adv. Organomet. Chem.* **2006**, *54*, 293.
(21) Deckers, P. J. W.; Hessen, B.; Teuben, J. H. *Organometallics* **2002**, *21*, 5122.

Scheme 1. Catalytic Cycle for Ethylene Trimerization by Cationic Cp-Arene Complexes of Titanium
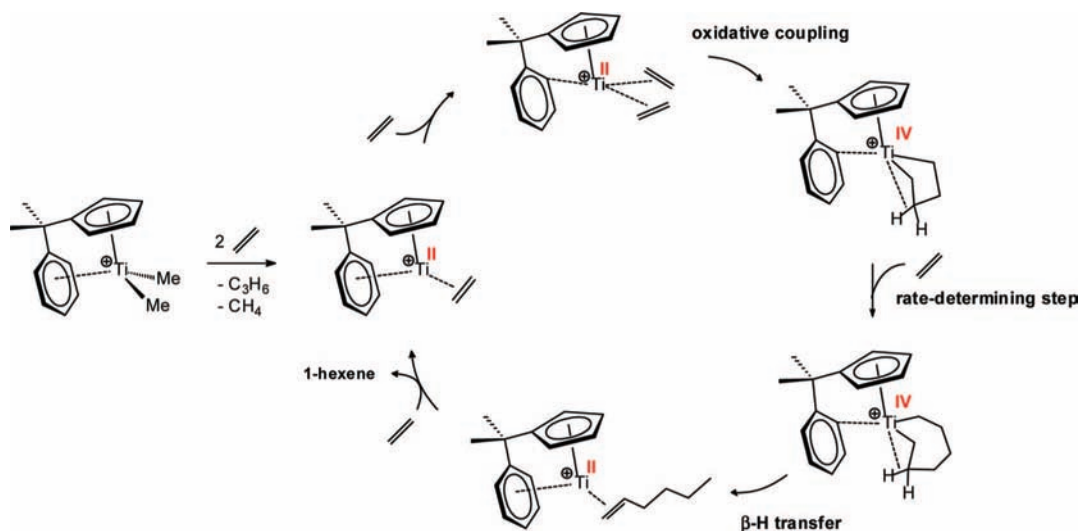
pendant donors were also shown to perform ethylene trimerization, but the activity of these is orders of magnitude lower than for the Cp-arene titanium systems.[23,24] Computational studies suggest that the pathway for ethylene trimerization occurs through a metallacyclic mechanism that involves Ti(II) and Ti(IV) intermediates.[25−27] This mechanism is analogous to that proposed for ethylene trimerization and tetramerization with chromium catalysts,[28−30] and involves initial oxidative coupling of two molecules of ethylene, followed by insertion of a third ethylene molecule, and a $C(\beta){\rightarrow}C(\alpha')$ hydrogen transfer (a net reductive elimination) to generate 1-hexene that is then liberated from the metal center (Scheme 1).

According to the calculations on the cyclopentadienyl-arene titanium catalyst system, the coordination of the pendant arene moiety (*ansa*-Cp-arene coordination mode) is instrumental in enabling this particular kind of catalysis, hitherto unknown for titanium. In particular, it appears that the role of the *ansa*-cyclopentadienyl-arene coordination mode of the ligand is 2-fold. On the one hand, the metal−arene interaction stabilizes the low-valent intermediates in the cycle, thereby enabling the reversible shuttling between Ti(IV) and Ti(II) oxidation states. At the same time, for the metallacyclic Ti(IV) intermediates, the arene coordination is sufficiently weak to give rise to *hemilabile* behavior, allowing slippage to a lower hapticity that enables ethylene coordination and subsequent insertion.
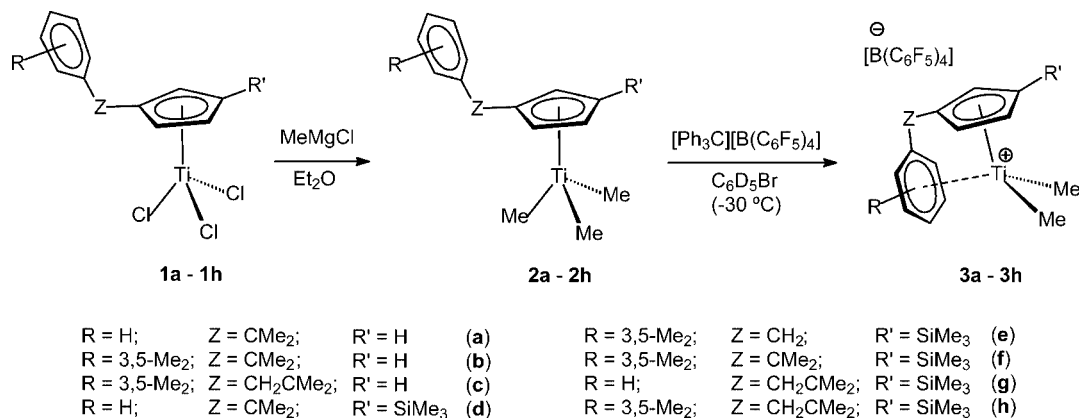
Reversible 2-electron redox processes, in particular reductive elimination reactions, are rare for the early transition metals (and certainly in catalytic processes) since the high-valent state is usually thermodynamically much more stable. Therefore,

classical C−C bond forming processes mediated by group 4 metals (e.g., Ziegler−Natta type polymerization) occur without changes of the oxidation state at the metal center. In contrast, many bond forming reactions catalyzed by late transition metals rely on a reductive elimination step to complete the catalytic cycle.[31−34] For the group 4 metal zirconium, R−H elimination from alkyl hydrido and aryl hydrido zirconocenes occurs by 'cyclometalation assisted' and direct reductive elimination pathways, respectively.[35,36] Recently, ligands that are able to function as an electron reservoir have received considerable attention as a means to support unusual redox chemistry.[37−41] By using this strategy, Heyduk and co-workers were able to effect the direct reductive elimination of biphenyl from a group 4 metal complex.[38] Previous studies in our group have shown that intramolecular coordination of the pendant arene moiety in cationic Cp-arene complexes of the group 5 metal tantalum gives rise to compounds that exhibit ambivalent [Ta(III)↔Ta(V)] character in their structural and reactive properties, by virtue of the redox behavior of the coordinated arene.[42]

The apparent ability of the hemilabile Cp-arene ligand to sustain the 2-electron redox switching that is necessary for titanium-catalyzed ethylene trimerization has prompted us to investigate experimentally the coordination behavior of the

(22) Deckers, P. J. W.; Hessen, B.; Teuben, J. H. *Angew. Chem., Int. Ed.* **2001**, *40*, 2516.
(23) Huang, J. L.; Wu, T. Z.; Qian, Y. L. *Chem. Commun.* **2003**, 2816.
(24) Wu, T.; Qian, Y.; Huang, J. *J. Mol. Catal. A: Chem.* **2004**, *214*, 227.
(25) Blok, A. N. J.; Budzelaar, P. H. M.; Gal, A. W. *Organometallics* **2003**, *22*, 2564.
(26) De Bruin, T. J. M.; Magna, L.; Raybaud, P.; Toulhoat, H. *Organometallics* **2003**, *22*, 3404.
(27) Tobisch, S.; Ziegler, T. *Organometallics* **2003**, *22*, 5392.
(28) Wass, D. F. *Dalton Trans.* **2007**, 816.
(29) Agapie, T.; Schofer, S. J.; Labinger, J. A.; Bercaw, J. E. *J. Am. Chem. Soc.* **2004**, *126*, 1304.
(30) Overett, M. J.; Blann, K.; Bollmann, A.; Dixon, J. T.; Haasbroek, D.; Killian, E.; Maumela, H.; McGuinness, D. S.; Morgan, D. H. *J. Am. Chem. Soc.* **2005**, *127*, 10723.

(31) Barrios-Landeros, F.; Hartwig, J. F. *J. Am. Chem. Soc.* **2005**, *127*, 6944.
(32) Espinet, P.; Echavarren, A. M. *Angew. Chem., Int. Ed.* **2004**, *43*, 4704.
(33) Negishi, E. I. *Handbook of Organopalladium Chemistry for Organic Synthesis*; Wiley-Interscience: New York, 2002.
(34) De Meijere, A.; Diederich, F. *Metal-Catalyzed Cross-Coupling Reactions*; Wiley-VCH: Weinheim, Germany, 2004; pp 1−40.
(35) Pool, J. A.; Lobkovsky, E.; Chirik, P. J. *J. Am. Chem. Soc.* **2003**, *125*, 2241.
(36) Bernskoetter, W. H.; Pool, J. A.; Lobkovsky, E.; Chirik, P. J. *Organometallics* **2006**, *25*, 1092.
(37) Blackmore, K. J.; Ziller, J. W.; Heyduk, A. F. *Inorg. Chem.* **2005**, *44*, 5559.
(38) Haneline, M. R.; Heyduk, A. F. *J. Am. Chem. Soc.* **2006**, *128*, 8410.
(39) Stanciu, C.; Jones, M. E.; Fanwick, P. E.; Abu-Omar, M. M. *J. Am. Chem. Soc.* **2007**, *129*, 12400.
(40) Bart, S. C.; Chlopek, K.; Bill, E.; Bouwkamp, M. W.; Lobkovsky, E.; Neese, F.; Wieghardt, K.; Chirik, P. J. *J. Am. Chem. Soc.* **2006**, *128*, 13901.
(41) Bouwkamp, M. W.; Bowman, A. C.; Lobkovsky, E.; Chirik, P. J. *J. Am. Chem. Soc.* **2006**, *128*, 13340.
(42) Otten, E.; Meetsma, A.; Hessen, B. *J. Am. Chem. Soc.* **2007**, *129*, 10100.

Scheme 2. Synthesis of Cationic *ansa*-Cp-Arene Complexes of Titanium(IV)

R = H;	Z = CMe₂;	R' = H	(a)

R = H;   Z = CMe₂;   R' = H   (a)
R = 3,5-Me₂;   Z = CMe₂;   R' = H   (b)
R = 3,5-Me₂;   Z = CH₂CMe₂;   R' = H   (c)
R = H;   Z = CMe₂;   R' = SiMe₃   (d)

R = 3,5-Me₂;   Z = CH₂;   R' = SiMe₃   (e)
R = 3,5-Me₂;   Z = CMe₂;   R' = SiMe₃   (f)
R = H;   Z = CH₂CMe₂;   R' = SiMe₃   (g)
R = 3,5-Me₂;   Z = CH₂CMe₂;   R' = SiMe₃   (h)

pendant arene moiety in systems that model the various intermediates in the catalytic cycle. We show how the metal−arene interaction strength modulates the activity in catalytic ethylene trimerization, and present structural and computational evidence for the versatile coordination behavior of the cyclopentadienyl-arene ligand.

Results and Discussion

Synthesis and X-ray Crystal Structures of [Cp-arene]TiMe₂⁺. The neutral trimethyl titanium compounds [Ar-Z-η^5-C₅H₃R]TiMe₃ (**2a−h**) are readily obtained by alkylation of the trichloride precursors (**1a−h**) using MeMgCl. Subsequent treatment with [Ph₃C][B(C₆F₅)₄] in bromobenzene at −30 °C gives dark orange solutions of the ionic compounds {[η^6-Ar-Z-η^5-C₅H₃R]TiMe₂}[B(C₆F₅)₄] (**3a−h**) (Scheme 2).[43,44] According to ¹H NMR spectroscopy, the conversion to the dimethyl cations is quantitative, with concomitant liberation of Ph₃CMe. The chemical shift difference between the Cp resonances increases on going from the trimethyl complexes **2a−h** to the cationic compounds **3a−h**, a feature that has been taken as an indication of strained *ansa*-Cp-arene coordination.[43] Consistently, this difference in chemical shift for the cations with a C₂ bridge (e.g., $\Delta\delta = 1.14$ ppm for **3c**) is smaller than in the complexes with a C₁ bridge ($\Delta\delta = 1.59$ ppm for **3b**). Arene complexes of d⁰ metal centers are rare, and structurally characterized *ansa*-Cp-arene coordination has only been reported for the d¹, Ti(III) dimer {[η^6-Ar-CMe₂-η^5-C₅H₄]Ti(μ-Br)⁺}₂.[44]

Slow interdiffusion of layered concentrated bromobenzene solutions of both reactants at −30 °C results in precipitation of orange crystals of **3a**, **3b**, and **3c** in 58, 64, and 96% isolated yield, respectively. The solubility of the SiMe₃-substituted compounds is significantly higher, but crystalline **3f** was obtained after diffusion of cyclohexane into the bromobenzene solution (78%). Single-crystal X-ray diffraction analysis yields the molecular structures shown in Figure 1, with pertinent interatomic distances and bond angles in Table 1.

The structure determination confirms the *ansa*-Cp-arene ligation in these complexes. For **3a**, disorder between the C₅ and C₆ ring precludes a fully satisfactory refinement. Nevertheless, it serves to establish that both rings are coordinated to the cationic titanium center.

The cationic part of **3b** shows a close resemblance to the neutral *ansa*-titanocene analogue Me₂C(C₅H₄)₂TiMe₂,[45] with a neutral arene (C₆) ring instead of one of the anionic cyclopentadienyl (C₅) ligands. The Cp(centroid)−Ti−Ar(centroid) angle of 123.24(7)° and the Cp-Ar interplanar angle (α) of 67.35° in **3b** are comparable to those in the C₁-bridged *ansa*-titanocene complex Me₂C(C₅H₄)₂TiMe₂ (Cp−Ti−Cp = 120.9°; α = 64.9°).[45] The angle between the Ti-Cp(centroid) vector and the ring normal (Cp tilt angle, τ_{Cp})[46] is 0.81° in **3b**, whereas the corresponding tilt angle for the arene ring (τ_{Ar}) is 9.91°. These values indicate that the binding of the neutral arene moiety is significantly more flexible compared to the anionic cyclopentadienyl ring, and suggest slippage to η^3-like arene coordination. This slippage is reflected in relatively short bonds between Ti and the *ipso*- and *ortho*-carbons of the coordinated arene (2.459(4)−2.559(3) Å) compared to those for the *meta*- and *para*-carbons (2.746(4)−2.830(4) Å), with $\Delta(d_{Ti−C})_{Ar} = 0.371$ Å ($\Delta(d_{Ti−C})_{Ar}$ is the difference between the longest and shortest Ti−C(arene) distance). Nevertheless, the planarity of the arene moiety in **3b** is preserved, with a maximum deviation from the least-squares plane of 0.011(3) Å for C(113). These metrical parameters are similar to those observed in the dimeric Ti(III) cation {[η^6-Ar-CMe₂-η^5-C₅H₄]Ti(μ-Br)⁺}₂,[44] although Ti−C(arene) distances in **3b** are on average ∼0.08 Å longer. Unbridged cationic analogues of **3b** are known for the group 4 triad in the form of (η^5-Cp′)(η^6-arene)MMe₂⁺, and X-ray structures are available for the hafnium congener (arene = toluene; Cp′ = C₅Me₅,[47] 1,3-C₅H₃(SiMe₃)₂[48]). These Hf compounds have a much smaller distribution in metal−C(arene) bond lengths ($\Delta(d_{Ti−C})_{Ar} = 0.098$ Å) and larger Cp(centroid)−M−Ar(centroid) angle of ∼134°, as expected in the absence of bridge-induced strain.

The C₂-bridged cation **3c** crystallizes with two independent molecules in the unit cell. The metrical parameters for these are similar, and only one of them will be discussed. The Ti−Ar(centroid) distance of 2.179(2) Å is shorter than in **3b** (2.2555(15) Å), and the largest difference in Ti−C(arene) bond distances ($\Delta(d_{Ti−C})_{Ar} = 0.163$ Å) is much smaller (0.371 Å for

(43) Sassmannshausen, J.; Powell, A. K.; Anson, C. E.; Wocadlo, S.; Bochmann, M. *J. Organomet. Chem.* **1999**, *592*, 84.
(44) Deckers, P. J. W.; van der Linden, A. J.; Meetsma, A.; Hessen, B. *Eur. J. Inorg. Chem.* **2000**, 929.

(45) Nifant'ev, I. E.; Churakov, A. V.; Urazowski, I. F.; Mkoyan, S.; Atovmyan, L. O. *J. Organomet. Chem.* **1992**, *435*, 37.
(46) Zachmanoglou, C. E.; Docrat, A.; Bridgewater, B. M.; Parkin, G.; Brandow, C. G.; Bercaw, J. E.; Jardine, C. N.; Lyall, M.; Green, J. C.; Keister, J. B. *J. Am. Chem. Soc.* **2002**, *124*, 9525.
(47) Gillis, D. J.; Quyoum, R.; Tudoret, M. J.; Wang, Q.; Jeremic, D.; Roszak, A. W.; Baird, M. C. *Organometallics* **1996**, *15*, 3600.
(48) Lancaster, S.; Robinson, O.; Bochmann, M.; Coles, S.; Hursthouse, M. *Organometallics* **1995**, *14*, 2456.
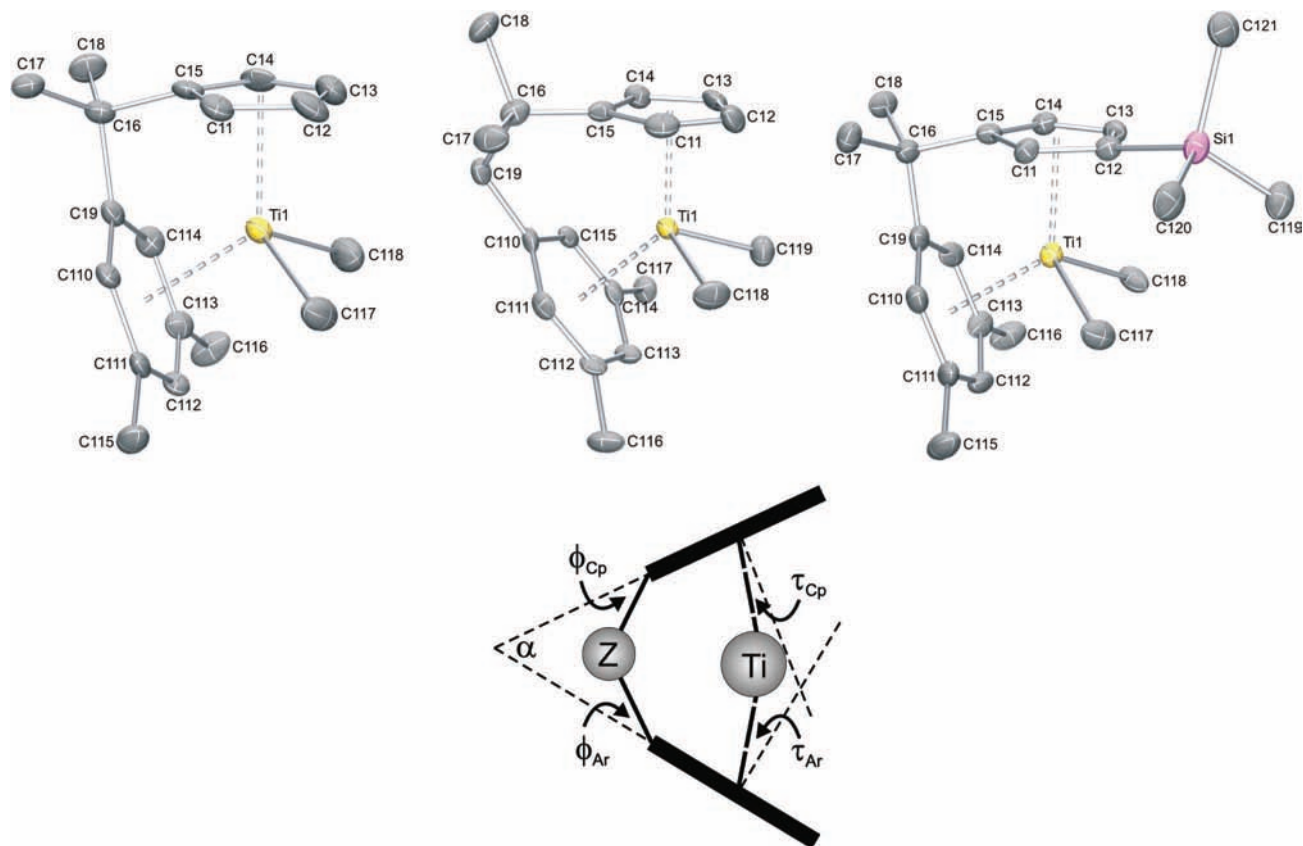
Figure 1. Molecular structures of **3b**, **3c** (one of the two independent molecules) and **3f** showing 50% probability ellipsoids (top). The B(C₆F₅)₄ anion and hydrogen atoms are omitted for clarity. Schematic representation of *ansa*-Cp-arene coordination, with definition of angles α, τ, and ϕ (bottom).

Table 1. Selected Bond Distances (Å) and Angles (deg) for **3b**, **3c**, and **3f**

	3b ($n = 0$)	**3c** ($n = 1$)	**3f** ($n = 0$)
Ti(1)−C(117+n)	2.128(5)	2.146(6)	2.129(5)
Ti(1)−C(118+n)	2.124(6)	2.134(6)	2.134(5)
Ti(1)−Cg(Cp)	2.0334(19)	2.042(3)	2.0435(18)
Ti(1)−C(11)	2.355(4)	2.369(6)	2.350(4)
Ti(1)−C(12)	2.379(5)	2.346(6)	2.413(4)
Ti(1)−C(13)	2.358(5)	2.372(6)	2.390(4)
Ti(1)−C(14)	2.347(4)	2.376(5)	2.351(4)
Ti(1)−C(15)	2.353(4)	2.386(5)	2.350(4)
Ti(1)−Cg(Ar)	2.2555(15)	2.179(2)	2.2102(18)
Ti(1)−C(19+n)	2.459(4)	2.533(5)	2.447(4)
Ti(1)−C(110+n)	2.521(4)	2.590(5)	2.553(5)
Ti(1)−C(111+n)	2.746(4)	2.668(5)	2.734(4)
Ti(1)−C(112+n)	2.830(4)	2.626(5)	2.760(4)
Ti(1)−C(113+n)	2.790(3)	2.612(5)	2.695(4)
Ti(1)−C(114+n)	2.559(3)	2.505(5)	2.494(4)
Δ($d_{Ti−C}$)$_{Cp}$[a]	0.032	0.040	0.063
Δ($d_{Ti−C}$)$_{Ar}$[a]	0.371	0.163	0.313
C(15)−C(16)−C(19)	97.0(3)		96.8(3)
Cg(Cp)−Ti(1)−Cg(Ar)	123.24(7)	130.88(10)	123.43(7)
α[b]	67.4(2)	51.8(3)	66.58(19)
ϕ$_{Cp}$[b]	15.3(3)	0.1(3)	14.1(2)
ϕ$_{Ar}$[b]	14.5(2)	3.7(3)	16.4(2)
τ$_{Cp}$[b]	0.80(19)	0.9(2)	1.78(16)
τ$_{Ar}$[b]	9.93(13)	3.69(18)	8.27(12)

[a] Δ($d_{Ti−C}$)$_{Cp}$/Δ($d_{Ti−C}$)$_{Ar}$ is the largest difference in Ti−C(arene)/ Ti−C(cyclopentadienyl) distances, respectively. [b] See Figure 1 for definition of angles.

3b), consistent with η⁶-arene coordination without significant ring slippage. The Cp(centroid)−Ti−Ar(centroid) angle of 130.88(10)° in **3c** approaches that of neutral (Cp₂TiCl₂: 131°)[49] or cationic (Cp′(toluene)HfMe₂⁺: 134°)[47,48] systems without

bridging atom between cyclopentadienyl and arene ligands. Introduction of a SiMe₃-substituent on the cyclopentadienyl ring (**3f**) results in a slightly more tilted cyclopentadienyl ring, due to the steric pressure exerted by the SiMe₃ group. As a result, the Ti−C(arene) distances in **3f** are slightly shorter than in **3b**, and more evenly distributed with Δ($d_{Ti−C}$)$_{Ar}$ = 0.313 Å.

Hemilabile Cp-Arene Coordination. Computational studies suggest that for ethylene trimerization catalysis by Cp-arene titanium catalysts, the rate-determining insertion of ethylene into the 5-membered metallacyle involves (partial) dissociation of the arene moiety.[25,27,50] To obtain insight into the factors that determine the strength of the metal−arene interaction in these systems, the dynamic behavior of the asymmetric complexes **3d−h** (Scheme 2) was studied by variable temperature NMR spectroscopy.

Cation **3f** (either isolated, or prepared *in situ* from **2f** and [Ph₃C][B(C₆F₅)₄] or [PhNMe₂H][B(C₆F₅)₄]) showed inequivalent ArMe ¹H NMR resonances (δ 2.09 and 2.06 ppm) at −25 °C in C₆D₅Br solution due to the asymmetry induced by the SiMe₃ substituent (Figure S1). Warming the solution of **3f** in the NMR spectrometer results in broadening of the ArMe signals, and coalescence is observed at 36.5 °C, resulting from rapid exchange of the arene enantiofaces through a dissociation−rotation−recoordination sequence (Scheme 3). Similarly, for the cations **3d−h**, variable-temperature NMR spectroscopy was performed to obtain the coalescence temperature for arene exchange, which allows a determination of the free energy of

(49) Clearfield, A.; Warner, D. K.; Saldarriagamolina, C. H.; Ropal, R.; Bernal, I. *Can. J. Chem.* **1975**, *53*, 1622.
(50) De Bruin, T. J. M.; Magna, L.; Raybaud, P.; Toulhoat, H. *Organometallics* **2003**, *22*, 3404.

Scheme 3. Arene Exchange (*Hemilabile* Behavior) in *ansa*-Cp-Arene Titanium Cations
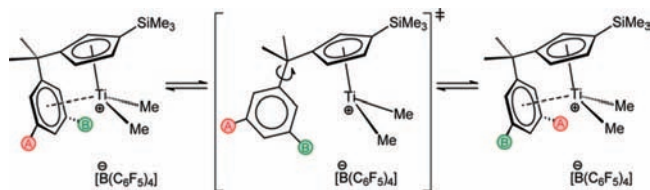
Table 2. Coalescence Temperature and Corresponding Activation Energy ($\Delta G^{\ddagger}_{Tc}$) for Site Exchange in **3d**−**3h**

cation[a]	arene	bridge	T_c (°C)[c]	$\Delta G^{\ddagger}_{Tc}$ (kJ·mol^{-1})
3d	Ph	CMe$_2$	<−60[b]	<45
3e	3,5-Me$_2$Ph	CH$_2$	−13.0	54.3(3)
3e[b]	3,5-Me$_2$Ph	CH$_2$	−3.0	57.1(4)
3f	3,5-Me$_2$Ph	CMe$_2$	36.5	67.0(6)
3g	Ph	CH$_2$CMe$_2$	>80	74(1)[d]
3h	3,5-Me$_2$Ph	CH$_2$CMe$_2$	>100	>81

[a] Generated in C$_6$D$_5$Br from **2d**−**2h** and [Ph$_3$C][B(C$_6$F$_5$)$_4$] at −30 °C, unless mentioned otherwise. [b] In CD$_2$Cl$_2$. [c] ±1 °C. [d] Value at 18.4 °C as determined by 2D EXSY NMR spectroscopy.

activation for the dynamic process.[51] It is presently unclear whether transient coordination of the anion or solvent is involved in this process. If this is the case, it is expected to affect the various derivatives in a comparable way. Data for the activation energy for arene exchange in **3d**−**h** are collected in Table 2.

For cation **3d**, the ^{1}H and ^{13}C NMR spectra exhibit equivalent *ortho*- and *meta*-CH groups for the pendant phenyl ring at all temperatures we examined (no decoalescence could be observed down to −60 °C in CD$_2$Cl$_2$). Conversely, the C$_2$-bridged cationic compounds **3g** and **3h** are static on the NMR time scale and show no evidence of coalescence up to temperatures where decomposition (to unidentified paramagnetic species) occurs. Nevertheless, for **3g** the *ortho*-CH resonances are sufficiently separated to allow determination of the free energy of activation by 2D EXSY NMR spectroscopy ($\Delta G^{\ddagger}$ = 74(1) kJ·mol^{-1} at 18.4 °C). A comparison of the activation energies in Table 2 shows that there is a significant influence of the electron-density in the arene moiety: the activation energy for site exchange is substantially larger when electron-donating methyl substituents are present (cf. 3,5-Me$_2$Ph (**3f/3h**) and Ph (**3d/3g**)), in line with computational[52] and experimental[47,53] work on related systems. Changing the nature of the bridge from CMe$_2$ (**3f**) to CH$_2$ (**3e**) results in a weaker Ti−arene interaction ($\Delta G^{\ddagger}_{Tc}$ = 54.3(3) kJ·mol^{-1} at −13.0 °C in C$_6$D$_5$Br). The stronger metal−arene interaction for **3f** is most likely the result of a smaller Cp(C$_{ipso}$)−C$_{bridge}$−Ar(C$_{ipso}$) angle compared to **3e**, due to increased steric interactions of the methyl substituents on the bridging carbon atom (Thorpe−Ingold effect).[54] The activation barrier for arene exchange in **3e** was shown to be slightly solvent-dependent, with $\Delta G^{\ddagger}_{Tc}$ = 57.1(4) kJ·mol^{-1} at −3.0 °C in CD$_2$Cl$_2$. Additionally, coalescence of the TiMe resonances was observed at +3 °C in CD$_2$Cl$_2$ ($\Delta G^{\ddagger}_{Tc}$ = 59.5(5) kJ·mol^{-1}). The exchange of the TiMe groups can only occur by inversion at the metal center, a process for which the arene moiety needs to be completely detached. Thus, there apparently is only a modest additional barrier of 2.4 kJ·mol^{-1} to inversion.

Table 3. Catalytic Ethylene Conversion with the **1**/MAO and **3** Catalyst Systems

catalyst[a]	C$_6$[b] (g)	PE (g)	C$_6$ selectivity (wt %)	C$_6$ productivity[c]
1d/MAO	12.5	0.21	98.3	997
1f/MAO	20.0	0.10	99.5	1602
1g/MAO	0.3	0.05	85.9	23
1h/MAO	none	0.17	−	−
3d	7.8	0.27	96.7	1045
3f	20.6	0.18	99.1	2747
3g	0.3	0.21	56.9	37
3h	none	0.27	−	−

[a] **1**: 5 μmol catalyst precursor, premixed with 250 equiv MAO, total 500 equiv MAO, 10 bar, 30 °C, 15 min. **3**: 3 μmol catalyst precursor (**2**), 1.05 equiv ammonium borate [R$_2$NMeH][B(C$_6$F$_5$)$_4$], 40 mg MAO as scavenger, 10 bar, 30 °C, 15 min. [b] >99% 1-hexene. [c] In g(C$_6$)·mmol(Ti)$^{-1}$·bar^{-1}·h^{-1}.

Catalytic Ethylene Trimerization. The cationic complexes **3**, either generated from the trichloride precursors **1** and MAO, or prepared *in situ* from **2** and [R$_3$NH][B(C$_6$F$_5$)$_4$] (R = C$_{16}$H$_{31}$−C$_{18}$H$_{35}$),[55] were tested in ethylene trimerization. For the runs using **1**/MAO, solutions of the catalyst precursors were 'premixed' with MAO to achieve (partial) alkylation before reaction with ethylene, a procedure that was shown to give improved trimerization activity in related systems.[55] Catalysts that feature a C$_1$ linker between the cyclopentadienyl and arene moieties are efficient ethylene trimerization catalysts, with productivities up to 2747 g (C$_6$)·mmol(Ti)$^{-1}$·bar^{-1}·h^{-1} for **3f** (Table 3). Although ligand substituent effects are nonadditive and there appears to be a delicate balance in activity and stability leading to optimal catalyst productivity,[21] it is clear that the hemilabile behavior of the pendant arene moiety is crucial to obtain a good catalyst: tight arene binding as in **3g/h** (*vide supra*) effectively quenches the reactivity.

Synthesis and X-ray Crystal Structure of {[Cp-arene]Ti-(CO)$_2$}$^+$. The proposed metallacyclic mechanism for ethylene trimerization by cationic cyclopentadienyl-arene complexes of titanium implicates low-valent titanium(II) species as key intermediates. Attempts to isolate or spectroscopically observe such titanium(II) olefin adducts were thus far not successful.[55] Neutral group 4 metallocene(II) complexes may be stabilized by coordination of π-acidic ligands (e.g., CO,[56,57] ethylene,[58] butadiene,[59] acetylene[60,61]) to give complexes with a bent metallocene structure. Reduction of metallocene(IV) dihalide precursors with Na/Hg or Mg in the presence of the desired π-acid provides a general entry into such compounds.[56] Alternatively, the dicarbonyl analogues may be prepared by carbonylation of metallocene dialkyl compounds. For example, reaction of Cp$_2$TiR$_2$ (R = CH$_2$Ph, Me) with CO forms Cp$_2$Ti(CO)$_2$ in good yields under mild conditions.[62−64] The

(51) Hesse, M; Meier, H; Zeeh, B. *Spectroscopic Methods in Organic Chemistry*; Georg Thieme Verlag: Stuttgart, New York, 1997; pp 95−100.
(52) Tobisch, S.; Ziegler, T. *Organometallics* **2004**, *23*, 4077.
(53) Hayes, P. G.; Piers, W. E.; Parvez, M. *Chem.-Eur. J.* **2007**, *13*, 2632.
(54) Jung, M. E.; Piizzi, G. *Chem. Rev.* **2005**, *105*, 1735.

(55) Hagen, H.; Kretschmer, W. P.; Van Buren, F. R.; Van Oeffelen, D. A. *J. Mol. Catal. A: Chem.* **2006**, *248*, 237.
(56) Sikora, D. J.; Macomber, D. W.; Rausch, M. D. *Adv. Organomet. Chem.* **1986**, *25*, 317.
(57) Hanna, T. E.; Lobkovsky, E.; Chirik, P. J. *J. Am. Chem. Soc.* **2006**, *128*, 6018.
(58) Cohen, S. A.; Auburn, P. R.; Bercaw, J. E. *J. Am. Chem. Soc.* **1983**, *105*, 1136.
(59) Erker, G.; Kehr, G.; Frohlich, R. *Adv. Organomet. Chem.* **2004**, *51*, 109.
(60) Rosenthal, U.; Burlakov, V. V.; Arndt, P.; Baumann, W.; Spannenberg, A. *Organometallics* **2003**, *22*, 884.
(61) Rosenthal, U.; Burlakov, V. V.; Arndt, P.; Baumann, W.; Spannenberg, A.; Shur, V. B. *Eur. J. Inorg. Chem.* **2004**, 4739.
(62) Fachinetti, G.; Floriani, C. *J. Chem. Soc., Chem. Commun.* **1972**, 654.
(63) Fachinetti, G.; Floriani, C. *J. Organomet. Chem.* **1974**, *71*, C5−C7.

Scheme 4. Synthesis of [*ansa*-Cp-arene]Ti(CO)$_2$$^+$ complexes
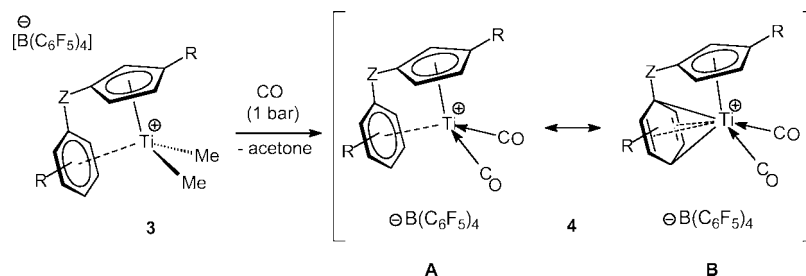
concomitant formation of the ketone $R_2C=O$ in these reactions suggests that the reaction proceeds *via* acyl intermediates. The analogy between neutral (*ansa*-)titanocene dialkyls and the *ansa*-Cp-arene titanium dimethyl cations discussed above prompted us to explore the carbonylation chemistry of **3**.

Reaction of the titanium(IV) dimethyl cations **3** with 1 bar of CO results in the formation of the cationic dicarbonyl species [η^6-Ar-Z-η^5-C$_5$H$_4$]Ti(CO)$_2$][B(C$_6$F$_5$)$_4$] (**4**) (Scheme 4). Monitoring the reaction of a representative C$_1$- (**3b**) and C$_2$-bridged compound (**3c**) with 1 bar of CO in C$_5$D$_5$Br solution by ^{1}H NMR spectroscopy shows that, while **3b** is fully consumed within 10 min, conversion of **3c** is slower and requires ∼3 h to go to completion. Although the reactions are not clean (see below), the dicarbonyl species are the major products (the side products have not been identified). Complex **4b** precipitates as red crystals from the C$_6$D$_5$Br solution upon standing at room temperature overnight. Alternatively, and with higher yield, **4b** is prepared by treatment of solid **3b** with excess CO. The orange color of the starting material gradually darkens to red in the course of 3 days, and ^{1}H NMR analysis of the crude reaction mixture indicates a greater purity compared to the analogous reaction in solution. The solid-state reaction for the C$_2$-bridged compound **3c**, however, proceeds much more slowly, reaching ∼35% conversion after a week at room temperature.

To determine the fate of the Ti−Me groups in **3b**, wet C$_6$D$_5$Br was added to an NMR tube containing the crude reaction mixture of the reaction of solid **3b** with CO (see Experimental Section for details). The ^{1}H NMR spectrum taken immediately after mixing showed the presence of **4b** and acetone (δ 1.81 ppm), in analogy to the carbonylation of dialkyl metallocenes of the group 4 triad.[56] When dry C$_6$D$_5$Br is added or when the reaction is carried out in dry C$_6$D$_5$Br solution, no acetone is observed. We propose that the acetone that is formed reacts with either starting material or product to give a (paramagnetic) product of unknown structure, but that this side product liberates acetone upon hydrolysis.

Single crystal X-ray analysis confirms **4b** to be the cationic dicarbonyl species {[η^6-Ar-CMe$_2$-η^5-C$_5$H$_4$]Ti(CO)$_2$][B(C$_6$F$_5$)$_4$] (Figure 2, pertinent interatomic distances and bond angles in Table 4). The *ansa*-Cp-arene ligation is similar to that observed in **3b**, but notable differences are observed in the metrical parameters of the coordinated C$_6$ ring. Unlike in **3b**, the arene ring in **4b** is significantly deformed from planarity, with folding along the C(19)−C(112) axis of 10.2(3)° and a Ti−C$_{para}$ bond (2.395(4) Å) that is *shorter* than the Ti−C$_{meta}$ distances (av. 2.472 Å). Moreover, the C$_{ortho}$−C$_{meta}$ distances in the ring are noticeably shorter (1.387(6) and 1.396(6) Å for C(110)−C(111) and C(113)−C(114), respectively) than the other C−C bonds

(64) Smith, J.; Von Seyerl, J.; Huttner, G.; Brintzinger, H. *J. Organomet. Chem.* **1979**, *173*, 175.

(av. 1.419 Å), which indicates a considerable degree of π-localization in the C$_6$ ring (Table 5).

The ^{1}H NMR spectrum of **4b** in C$_6$D$_5$Br is consistent with a C_s symmetric compound, and shows resonances for the arene moiety at δ 5.00 (*p*-H) and 4.38 ppm (*o*-H). The corresponding signals in **3b** are found at δ 7.02 and 5.91 ppm, respectively.[44] Also, in the ^{13}C NMR spectrum of **4b** the resonances for the C$_6$ ring are located significantly upfield from the aromatic region (δ 102.6/100.3/86.8 ppm for C$_{ortho}$/C$_{para}$/C$_{ipso}$). In accordance with crystallographic data, the upfield shift for the arene resonances suggests (at least partial) reduction of the arene ring in **4b**. Taken together, these data are indicative of contribution of the Ti(IV)/dienediyl resonance structure depicted in Scheme 4 (structure **B**).

A few related 'unbridged' arene complexes of group 4 metals have been reported and show substantially larger fold angles in
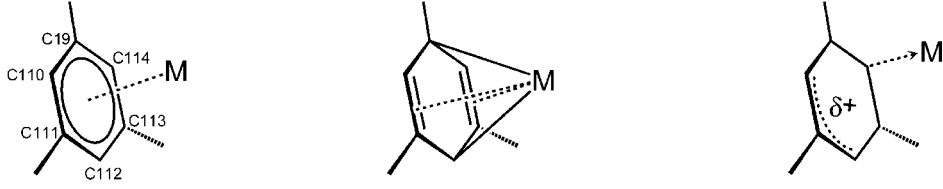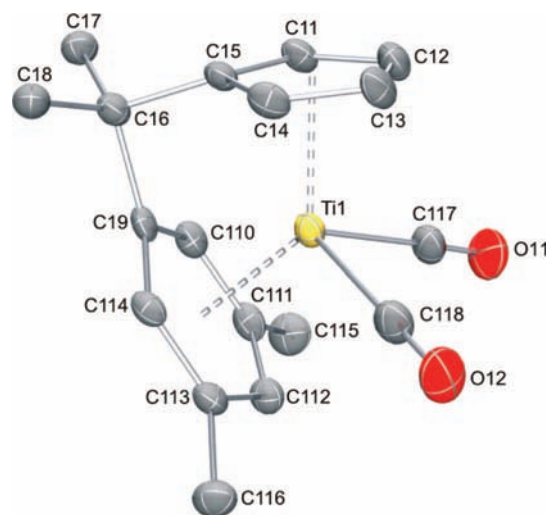

Figure 2. Molecular structure of **4b** showing 50% probability ellipsoids. The B(C$_6$F$_5$)$_4$ anion and hydrogen atoms are omitted for clarity.

Table 4. Selected Bond Distances (Å) and Angles (deg) for **4b**

Ti(1)−C(117)	2.091(5)	C(117)−O(11)	1.135(5)
Ti(1)−C(118)	2.100(5)	C(118)−O(12)	1.129(6)
Ti(1)−Cg(Cp)	1.994(2)	Ti(1)−Cg(Ar)	1.9341(16)
Ti(1)−C(11)	2.291(5)	Ti(1)−C(19)	2.264(4)
Ti(1)−C(12)	2.382(4)	Ti(1)−C(110)	2.372(4)
Ti(1)−C(13)	2.391(4)	Ti(1)−C(111)	2.466(3)
Ti(1)−C(14)	2.299(5)	Ti(1)−C(112)	2.395(4)
Ti(1)−C(15)	2.270(3)	Ti(1)−C(113)	2.478(4)
C(15)−C(16)−C(19)	94.3(3)	Ti(1)−C(114)	2.373(4)
Cg(Cp)−Ti(1)−Cg(Ar)	130.60(8)	α^a	57.6(3)
$\phi_{Cp}{}^a$	15.3(3)	$\phi_{Ar}{}^a$	21.8(2)
$\tau_{Cp}{}^a$	4.2(2)	$\tau_{Ar}{}^a$	3.99(13)

^{a} See Figure 1 for definition of angles.

Table 5. Comparison of Experimental and Calculated Arene C—C Bond Distances (Å) and Fold Angles (deg) in *ansa*-Cp-Arene Cations with C$_1$ Bridge[a]

	3b	3b[c]	4b	4b[c]	7b	7b[c]
C(19)—C(110)	1.409(5)	1.409	1.425(4)	1.425	1.387(3)	1.390
C(110)—C(111)	1.402(5)	1.409	1.387(6)	1.399	1.394(3)	1.403
C(111)—C(112)	1.383(5)	1.400	1.419(7)	1.420	1.383(3)	1.400
C(112)—C(113)	1.380(5)	1.399	1.412(4)	1.420	1.389(3)	1.390
C(113)—C(114)	1.414(5)	1.409	1.396(6)	1.399	1.408(3)	1.419
C(114)—C(19)	1.410(5)	1.408	1.421(7)	1.425	1.417(3)	1.424
ring folding[b]	0.3(3)	1.19	10.2(3)	11.58	1.41(16)	0.24

[a] **3b** [η^6-Me$_2$Ph-CMe$_2$-η^5-C$_5$H$_4$]TiMe$_2^+$; **4b** [η^6-Me$_2$Ph-CMe$_2$-η^5-C$_5$H$_4$]Ti(CO)$_2^+$; **7b** [η^1-Me$_2$Ph-CMe$_2$-η^5-C$_5$H$_4$]V(N^{i}Pr$_2$)(NC$_6$H$_4$-4-Me)$^+$ (see below). [b] Folding along the C(19)—C(112) axis. [c] DFT optimized geometry; see below.

the range of 20−30°.[65−68] Stephan and co-workers have shown that Mg reduction of the phosphinimide complexes Cp′Ti-[NP^{t}Bu$_2$(2-biphenyl)] (Cp′ = Cp, Cp*) results in complexes that coordinate the pendant arene ring of the biphenyl substituent. In these compounds, the fold angle (25.3−25.9°) is consistent with a Ti(IV)/reduced arene formulation.[69] The strained *ansa*-Cp-arene coordination in **4b** (evident from the very acute C(15)−C(16)−C(19) angle of 94.3(3)°) precludes optimal overlap between metal d- and arene π^*-orbitals. Consequently, the degree of reduction of the arene is lower than that of titanium(II) species without strained arene coordination.[42]

For the carbonyl ligands in **4b**, the crystallographic C−O bond lengths (1.129(6) and 1.135(5) Å) are virtually identical to the corresponding distances in typical Ti(II) systems (e.g., Me$_2$Si(C$_5$Me$_4$)$_2$Ti(CO)$_2$, C−O: 1.134(9) and 1.129(11) Å), and the Ti−C(carbonyl) distances are marginally longer (2.017(8) and 2.040(9) Å in **4b** versus 2.091(5) and 2.100(5) Å in Me$_2$Si(C$_5$Me$_4$)$_2$Ti(CO)$_2$).[70] In the ^{13}C NMR spectrum of **4b**, the signal for the CO ligands is observed at δ 227.3 ppm. This is intermediate between the ^{13}C NMR resonances of the carbonyl groups in d^2 titanocenes (Cp$_2$Ti(CO)$_2$: δ 260.5 ppm)[71] and free CO (δ 184.5 ppm in toluene-d$_8$ solution).[72] In the IR spectrum of **4b** two bands are observed at 2055 and 2022 cm^{-1} for the symmetric and antisymmetric CO stretching vibrations, respectively. Although lower than free CO (2143 cm^{-1}), these values are significantly higher than those found for typical d^2 titanocenes (Table 6). Conversely, stable d^0 metal complexes with CO ligands are rare, due to the lack of stabilizing M→CO π-backbonding interactions.[73,74] In cases when isolable adducts are formed, these are usually stabilized by donation from a metal−ligand σ-orbital into the CO π^*-orbital (σ→π^* backbond-

Table 6. Infrared Frequencies of CO Ligands in Representative Group 4 Metal Complexes

	v(CO) (cm^{-1})	v(CO)$_{av}$ (cm^{-1})	ref
Cp$_2$Ti(CO)$_2$	1977, 1899	1938	84
Me$_2$Si(C$_5$H$_5$)$_2$Ti(CO)$_2$	1980, 1905	1942.5	85
Cp$_2$TiCl(CO)		2068	86
[Cp*$_2$Zr(C$_3$H$_5$)(CO)]$^+$		2079	78
[Cp$_3$Zr(CO)]$^+$		2132/2150	87,88
[Cp$_2$Ti(CO)$_2$]$^{2+}$	2119, 2099	2109	88,89
Cp*$_2$ZrH$_2$(CO)		2044	76
4b	2055, 2022	2039	this work

ing).[75−83] A comparison of representative group 4 metal carbonyl adducts is collected in Table 6, showing that, in agreement with the structural features of the coordinated arene, compound **4b** is best described by significant contribution of resonance structure **B** (Scheme 4).[42]

Unfortunately, with the exception of **4b**, the *ansa*-Cp-arene titanium dicarbonyl compounds could not be crystallized, preventing isolation of the complexes in analytically pure form. Therefore, these compounds were generated on NMR tube scale in C$_6$D$_5$Br solution and the crude products were characterized by NMR and IR spectroscopic methods. For each compound, ^{1}H NMR spectroscopy shows resonances of the coordinated arene moiety in the range of δ 5.5−4 ppm, indicative of partial reduction of the C$_6$ ring. As anticipated, the Me$_3$Si-substituted compounds **4d−f,h** are asymmetric and show two sets of signals for both the *ortho* and *meta* substituents of the C$_6$ ring. At room temperature, the sharp and inequivalent *ortho*-H resonances

(65) Hagadorn, J. R.; Arnold, J. *Angew. Chem., Int. Ed.* **1998**, *37*, 1729.
(66) Ozerov, O. V.; Patrick, B. O.; Ladipo, F. T. *J. Am. Chem. Soc.* **2000**, *122*, 6423.
(67) Fryzuk, M. D.; Kozak, C. M.; Mehrkhodavandi, P.; Morello, L.; Patrick, B. O.; Rettig, S. J. *J. Am. Chem. Soc.* **2002**, *124*, 516.
(68) Kissounko, D.; Epshteyn, A.; Fettinger, J. C.; Sita, L. R. *Organometallics* **2006**, *25*, 531.
(69) Graham, T. W.; Kickham, J.; Courtenay, S.; Wei, P.; Stephan, D. W. *Organometallics* **2004**, *23*, 3309.
(70) Lee, H.; Bonanno, J. B.; Hascall, T.; Cordaro, J.; Hahn, J. M.; Parkin, G. *J. Chem. Soc., Dalton Trans.* **1999**, 1365.
(71) Kool, L. B.; Rausch, M. D.; Alt, H. G.; Herberhold, M.; Wolf, B.; Thewalt, U. *J. Organomet. Chem.* **1985**, *297*, 159.
(72) Kalodimos, C. G.; Gerothanassis, I. P.; Pierattelli, R.; Ancian, B. *Inorg. Chem.* **1999**, *38*, 4283.

(73) Lupinetti, A. J.; Strauss, S. H.; Frenking, G. *Prog. Inorg. Chem.* **2001**, *49*, 1.
(74) Dias, H. V. R.; Fianchini, M. *Angew. Chem., Int. Ed.* **2007**, *46*, 2188.
(75) Brintzinger, H. H. *J. Organomet. Chem.* **1979**, *171*, 337.
(76) Marsella, J.; Curtis, C.; Bercaw, J.; Caulton, K. *J. Am. Chem. Soc.* **1980**, *102*, 7244.
(77) Guram, A. S.; Swenson, D. C.; Jordan, R. F. *J. Am. Chem. Soc.* **1992**, *114*, 8991.
(78) Antonelli, D.; Tjaden, E.; Stryker, J. *Organometallics* **1994**, *13*, 763.
(79) Guo, Z.; Swenson, D.; Guram, A.; Jordan, R. *Organometallics* **1994**, *13*, 766.
(80) Procopio, L. J.; Carroll, P. J.; Berry, D. H. *Polyhedron* **1995**, *14*, 45.
(81) Howard, W. A.; Parkin, G.; Rheingold, A. L. *Polyhedron* **1995**, *14*, 25.
(82) Howard, W. A.; Trnka, T. M.; Parkin, G. *Organometallics* **1995**, *14*, 4037.
(83) Burckhardt, U.; Tilley, T. D. *J. Am. Chem. Soc.* **1999**, *121*, 6328.

Table 7. Average ^{13}C NMR Shift and Infrared Frequencies of CO Ligands in **4**

	δ (CO)$_{av}$ (ppm)	v(CO) (cm^{-1})	v(CO)$_{av}$ (cm^{-1})	v(CO)$_{av,calc}$^{b} (cm^{-1})
4a	226.6	2064, 2032	2048	2058
4b	227.3	2055, 2022	2039	2047
4c	237.0	2039, 1997	2018	2032
4d	^{c}	2056, 2022	2039	2046
4e	229.9	2047, 2010	2029	^{c}
4f	229.2	2048, 2012	2030	2036
4h	238.3	2033, 1989	2011	2021
Cp$_2$Ti(CO)$_2$^{a}	260.5	1977, 1899	1938	1964

^{a} Reference 84. ^{b} Calculated frequencies after scaling by a factor of 0.97.[90,91] ^{c} Not determined

(**4f**: δ 4.41 and 4.38 ppm) indicate that arene exchange such as observed for **3f** is slow on the NMR time scale. Upon heating to 80 °C no line broadening is observed, from which we conclude that, in contrast to the titanium(IV) dimethyl cations described above, the *ansa*-Cp-arene ligands in the dicarbonyl compounds **4** no longer exhibit hemilabile behavior. This is likely due to the partial reduction of the arene in these complexes, leading to a much stronger metal−arene interaction than for titanium(IV) complexes.

The infrared spectra of the crude reaction mixtures show only two bands in the region 1800−2200 cm^{-1} that are attributed to CO vibrations of the dicarbonyl cations. Apparently, other species that are present in the crude mixture do not contain terminal CO ligands, and a comparison of the carbonyl ^{13}C NMR and IR frequencies is appropriate (Table 7). There is a significant decrease of ∼20 cm^{-1} in the observed CO absorption frequency upon increasing the bridge length by one carbon atom (**4b** vs **4c** and **4f** vs **4h**). The increased electron density in the arene ring by adding methyl substituents (Ph in **4a/d** vs 3,5-Me$_2$Ph in **4b/f**) is seen to lower the average CO frequency by 9 cm^{-1}. A similar effect is observed for the SiMe$_3$-substituent on the cyclopentadienyl ring, which results in a lowering of v(CO)$_{av}$ by 7−9 cm^{-1} (cf. **4b** and **4f**). The latter is probably not related to an inductive effect of the SiMe$_3$ group, since this is shown to be very small (∼1.5 cm^{-1}) in ziroconocene dicarbonyls.[46] Instead, the steric pressure exerted by the SiMe$_3$ group results in tilting of the cyclopentadienyl ring, which allows a closer approach of the arene moiety to the metal center (see X-ray structure of **3f** above). Calculated IR frequencies (using density functional theory, *vide infra*) corroborate the experimental trend (Table 7). It thus appears that the σ-donor capacity of the pendant arene group is more important than its π-acceptor properties in modulating the electron density at the metal center.

Synthesis and X-ray Crystal Structure of *ansa*-Cp-Arene Complexes of Vanadium(V). Computational studies on the catalytic ethylene trimerization cycle have shown that slippage

to η^1-coordination of the pendant arene moiety occurs when the steric and/or electronic unsaturation at the metal center is alleviated, either by agostic interactions with CH$_2$ units of the metallacycle or by coordination of ethylene.[27] To test this idea, we have prepared the vanadium compounds [Ar-Z-η^5-C$_5$H$_4$]VMe(N^{i}Pr$_2$)(NC$_6$H$_4$-4-Me) (Z = CMe$_2$, **6b**; CH$_2$CMe$_2$, **6c**) by alkylation of the dichloride precursors **5b/c** using MeLi. The electron-deficiency of the metal in these compounds is compensated for by π-charging through the lone pairs of the amido and imido ligands. Treatment of **6b/c** with the Lewis acid [Ph$_3$C][B(C$_6$F$_5$)$_4$] in dichloromethane results in formation of the ionic complexes {[η^1-Ar-Z-η^5-C$_5$H$_4$]V(N^{i}Pr$_2$)(NC$_6$H$_4$-4-Me)}-[B(C$_6$F$_5$)$_4$] (**7b/c**) (Scheme 5). The structure of **7b** was confirmed by X-ray analysis (Figure 3, pertinent intermolecular distances and bond angles in Table 8).

The cationic vanadium center is coordinated by a diisopropylamido ligand and a slightly bent *p*-tolylimido group (V(1)−N(11)−C(117) = 157.85(15)°). The salient structural feature of **7b** is the bonding of the arene moiety of the Cp-arene ligand. One of the *ortho* positions shows a close approach to the metal center (V(1)−C(114) = 2.411(2) Å), whereas the other C(arene) atoms are much further away (Table 8), resulting in a complex with *ansa*-(η^5-C$_5$H$_4$,η^1-arene) coordination mode. The C(15)−C(16)−C(19) angle of 102.76(17)° indicates release of conformational strain compared to **3b** and **4b** as a result of slippage to η^1-arene coordination. The arene ring is nearly planar, with a largest displacement from the least-squares plane of 0.020(2) Å for C(114). The ring C−C bond lengths to the coordinated *ortho*-CH group (1.417(3) and 1.408(3) Å for C(19)−C(114) and C(113)−C(114), respectively) are longer than the remaining C−C bonds (av. 1.388 Å), and the C−H bond deviates from the C$_6$-plane by 9.7(16)°, as is observed for η^1-arene complexes of moderately strong Lewis acids (π-/σ-intermediate bonding).[92] A comparison of the C−C bond lengths within the coordinated C$_6$ ring in **3b**, **4b**, and **7b** is presented in Table 5. Related η^1-arene binding of a pendant *p*-tolyl group has recently been inferred from spectroscopic and computational studies on the zirconocene cation [η^1-(4-Me-C$_6$H$_4$)-CMe$_2$-η^5-C$_5$H$_4$]CpZr(CH$_2$Ph)$^+$.[93]

For **7b/c**, ^{1}H NMR spectroscopy at 500 MHz in CD$_2$Cl$_2$ at room temperature shows broad resonances for the *o*-CH and *m*-Me groups of the arene moiety due to dynamic exchange, while the remaining signals do not exhibit line broadening. Below 0 °C, the ^{1}H NMR spectra are sharp, and the number of resonances is consistent with the C_1 symmetric structure observed in the solid state. The *ortho*-protons of the pendant arene moiety are inequivalent and observed at δ 7.01/5.25 and 7.04/5.55 ppm for **7b** and **7c**, respectively. Exchange between these resonances was confirmed by 2D EXSY NMR spectroscopy. Analysis of EXSY spectra obtained at four different temperatures between −25 and +10 °C gives the activation parameters for the dynamic process as $\Delta H^\ddagger$ = 63.7(7) kJ·mol^{-1} and $\Delta S^\ddagger$ = 7(3) J·mol^{-1}·K^{-1} for **7b**. A similar analysis for **7c** affords comparable values of $\Delta H^\ddagger$ = 61.1(9) kJ·mol^{-1} and $\Delta S^\ddagger$ = 5(4) J·mol^{-1}·K^{-1}, indicating that the strength of the η^1-arene interaction is relatively insensitive to the length of the bridge. The small and positive values for $\Delta S^\ddagger$ are consistent with an intramolecular process involving at least partial detachment of the arene moiety in the transition state. Extrapolation to 36.5

(84) Sikora, D.; Rausch, M.; Rogers, R.; Atwood, J. *J. Am. Chem. Soc.* **1981**, *103*, 1265.

(85) Cuenca, T.; Gomez, R.; Gomez-Sal, P.; Royo, P. *J. Organomet. Chem.* **1993**, *454*, 105.

(86) Van Raaij, E. U.; Schmulbach, C. D.; Brintzinger, H. H. *J. Organomet. Chem.* **1987**, *328*, 275.

(87) Brackemeyer, T.; Erker, G.; Frohlich, R. *Organometallics* **1997**, *16*, 531.

(88) Pampaloni, G.; Tripepi, G. *J. Organomet. Chem.* **2000**, *593−594*, 19.

(89) Calderazzo, F.; Pampaloni, G.; Tripepi, G. *Organometallics* **1997**, *16*, 4943.

(90) Jang, J. H.; Lee, J. G.; Lee, H.; Xie, Y.; Schaefer, H. F. *J. Phys. Chem. A* **1998**, *102*, 5298.

(91) Koch, W.; Holthausen, M. C. *A Chemist's Guide to Density Functional Theory*; Wiley-VCH: Weinheim, 2002; pp 130−136.

(92) Hubig, S. M.; Lindeman, S. V.; Kochi, J. K. *Coord. Chem. Rev.* **2000**, *200−202*, 831.

(93) Sassmannshausen, J.; Track, A.; Dias, T. A. D. S. *Eur. J. Inorg. Chem.* **2007**, 2327.

Scheme 5. Synthesis of {[η^1-Ar-Z-η^5-C$_5$H$_4$]V(N^{i}Pr$_2$)(NC$_6$H$_4$-4-Me)}[B(C$_6$F$_5$)$_4$] (**7b/c**)

5b (Z = CMe$_2$)
5c (Z = CH$_2$CMe$_2$)   6b/c   7b/c
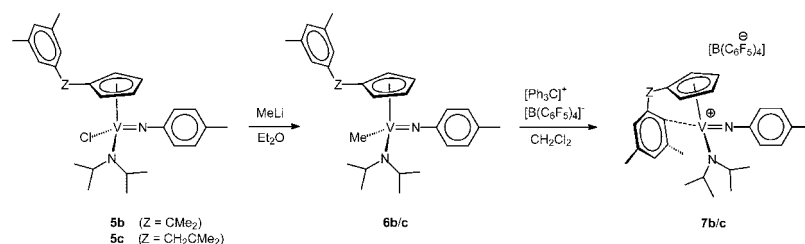
°C (the coalescence temperature for **3f**) gives arene exchange activation energies of $\Delta G^{\ddagger} = 62(1)$ and $60(2)$ kJ·mol^{-1} for the η^1-arene cations **7b** and **7c**, respectively, which compares to $67.0(6)$ kJ·mol^{-1} for the η^6-arene cation **3f**.

Computational Studies. The *ansa*-Cp-arene cations were studied by DFT calculations (the anions were omitted, see Experimental Section for details). A series of computational papers has appeared that focuses on the energetic landscape of titanium-catalyzed ethylene trimerization,[25,27,94] the influence of changing the metal center to Zr/Hf,[52,95] as well as differences in ligand architecture.[52,119] With the crystallographic characterization of compounds that model key species in the catalytic cycle in hand, we feel that a detailed analysis of the factors governing the metal−arene interaction by computational methods is appropriate. Specifically, we explore the differences between the η^6-arene Ti(IV) and Ti(II) cations, the η^1-arene V(V) cation, and the influence of the bridge length on the metal−arene interaction.

The optimized structures of the cationic titanium complexes adopt the *ansa*-Cp-arene coordination geometry, in overall agreement with the X-ray crystal structures described above.
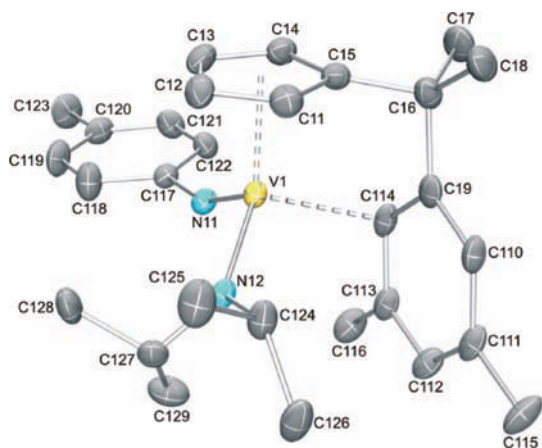
Figure 3. Molecular structure of **7b**, showing 50% probability ellipsoids.; the B(C$_6$F$_5$)$_4$ anion and hydrogen atoms are omitted for clarity

Table 8. Selected Bond Distances (Å) and Angles (deg) for **7b**

V(1)−N(11)	1.6774(17)	V(1)−N(12)	1.8699(17)
V(1)−Cg(Cp)	1.9674(11)	V(1)−Cg(Ar)	3.1534(11)
V(1)−C(11)	2.326(2)	V(1)−C(19)	2.876(2)
V(1)−C(12)	2.269(2)	V(1)−C(110)	3.752(2)
V(1)−C(13)	2.282(2)	V(1)−C(111)	4.225(2)
V(1)−C(14)	2.307(2)	V(1)−C(112)	3.950(2)
V(1)−C(15)	2.336(2)	V(1)−C(113)	3.122(2)
C(15)−C(16)−C(19)	102.76(17)	V(1)−C(114)	2.411(2)
Cg(Cp)−V(1)−Cg(Ar)	110.37(4)	α^a	86.86(11)
$\phi_{Cp}{}^a$	9.51(15)	$\phi_{Ar}{}^a$	0.66(13)
$\tau_{Cp}{}^a$	1.85(9)	$\tau_{Ar}{}^a$	43.53(7)

^{a} See Figure 1 for definition of angles.

The main difference lies in the Ti−C(arene) bond distances, which are on average larger by 0.16 and 0.14 Å for the calculated cations **3b′** and **3c′** in comparison to the crystal structures of **3b** and **3c**, respectively. The energy associated with this elongation is small: the calculated energy of **3b′** using Ti−C(arene) bond lengths found in the X-ray structure is only 1.3 kcal·mol^{-1} higher in energy. For the dicarbonyl compound **4b**, the DFT optimized structure (**4b′**) is in good agreement with that found by X-ray crystallography, with Ti−C(arene) distances that are only slightly longer by ∼0.05 Å. Importantly, while the arene moieties in the optimized structures of the dimethyl cations **3b′/3c′** are nearly planar, the C−C bonds within the arene group of **4b′** manifest a similar degree of π-localization as found in the X-ray structure (see Table 5); in addition, the ring is folded by 11.6° (X-ray structure: 10.2(3)°). The calculated Ti−C(carbonyl) and C−O bond lengths for **4b′** are 2.087 and 1.137 Å, respectively (for **4a′−d′**, see Table S1), which is comparable to the values found by the crystal structure determination (Ti−C(carbonyl): 2.091(5)/2.100(5); C−O: 1.135(5)/1.129(6) Å). In addition, the calculated CO stretching frequencies for these dicarbonyl species follow the same trend as observed experimentally (Table 7). The corresponding bond lengths calculated for Cp$_2$Ti(CO)$_2$ using the same DFT method are substantially different, with a Ti−C(carbonyl) distance of 2.039 Å and a C−O bond length of 1.150 Å (Table S1). The experimentally observed singlet ground-state for **4b′** is also obtained computationally: a triplet state with a more planar arene moiety (fold angle = 4.69°) is calculated to be 17.3 kcal·mol^{-1} higher in energy.

Geometry optimization of a simplified model of vanadium cation **7b′** (with Me substituents on the amido and C$_6$H$_5$ on the imido ligand) converged at a structure that is similar to the one obtained by X-ray crystallography, including the η^1-arene coordination (Figure 4). This shows that the η^1-arene coordination in the crystallographically determined structure of **7b** is not enforced by the steric demand of the diisopropyl amido ligand, but instead is due to the more electron-rich metal center compared to the η^6-coordinated Ti(IV) cation **3b**.
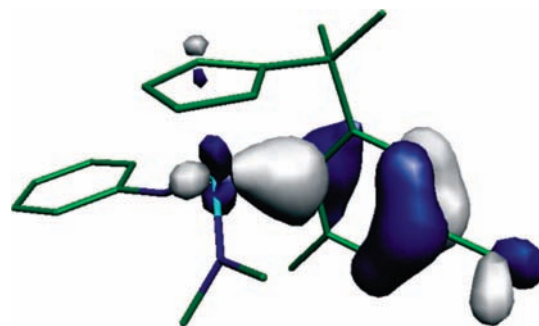
Figure 4. Optimized structure of simplified model for **7b′**, showing the orbital (HOMO−4) involved in η^1-arene coordination.
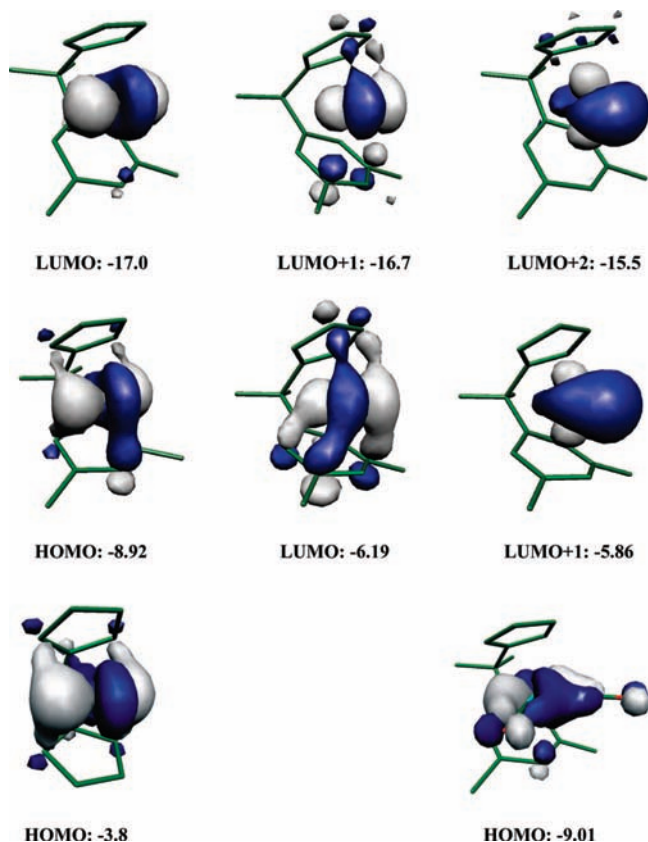
Figure 5. Frontier molecular orbitals of $[\eta^6\text{-Ar-CMe}_2\text{-}\eta^5\text{-C}_5\text{H}_4]\text{Ti}^{3+}$ (**Ti(b)**$^{3+}$, top) and $[\eta^6\text{-Ar-CMe}_2\text{-}\eta^5\text{-C}_5\text{H}_4]\text{Ti}^+$ (**Ti(b)**$^+$, middle), HOMO of $\text{H}_2\text{C(C}_5\text{H}_4)_2\text{Ti}$ (bottom left), HOMO of $[\eta^6\text{-Ar-CMe}_2\text{-}\eta^5\text{-C}_5\text{H}_4]\text{Ti(CO)}_2^+$ (**4b′**, bottom right) and their corresponding energies (eV).

Table 9. Percentage Contributions of Different Fragments to the Highest Occupied Molecular Orbital in Titanium(II) Compounds (Or the Equivalent Orbital (LUMO) in Case of the Titanium(IV) Species **Ti(b)**$^{3+}$ and $\text{H}_2\text{C}(\eta^5\text{-C}_5\text{H}_4)_2\text{Ti}^{2+}$)

	Ti	Cp	arene	(CO)$_2$
Ti(b)$^{3+}$	82	8	11	
Ti(b)$^+$	61	11	28	
Ti(c)$^+$	62	8	30	
$\text{H}_2\text{C(C}_5\text{H}_4)_2\text{Ti}^{2+}$	80	10 + 10		
$\text{H}_2\text{C(C}_5\text{H}_4)_2\text{Ti}$	72	14 + 13		
4b′	57	6	15	22
4c′	58	5	13	24
$\text{H}_2\text{C(C}_5\text{H}_4)_2\text{Ti(CO)}_2$	58	6 + 6		30

Analysis of the frontier molecular orbitals shows the isolobal relationship between the 'naked' cationic Ti(IV)/Ti(II) fragments $[\eta^6\text{-Ar-CMe}_2\text{-}\eta^5\text{-C}_5\text{H}_4]\text{Ti}^{3+}$ (**Ti(b)**$^{3+}$)/$[\eta^6\text{-Ar-CMe}_2\text{-}\eta^5\text{-C}_5\text{H}_4]\text{Ti}^+$ (**Ti(b)**$^+$) and the well-known bent metallocenes (Figure 5).[96,97] The HOMO of these is the equivalent of the 1a$_1$ orbital in C_{2v} symmetric bent metallocenes and for the titanium(II) cation **Ti(b)**$^+$ consists mainly (82%) of titanium based atomic orbitals (Table 9), indicating appreciable Ti(II), d^2 character. The major ligand contribution to the HOMO comes from the arene moiety (28%). The C$_2$-bridged system $[\eta^6\text{-Ar-CH}_2\text{CMe}_2\text{-}\eta^5\text{-C}_5\text{H}_4]\text{Ti}^+$ (**Ti(c)**$^+$) has a similar frontier orbital structure, with comparable energies (Figure S1). For comparison, we have calculated the

structure of the analogous 'naked' neutral *ansa*-titanocene complex $\text{H}_2\text{C(C}_5\text{H}_4)_2\text{Ti}$ at the same level of theory (Figure 5). The energy of the frontier molecular orbitals in $\text{H}_2\text{C(C}_5\text{H}_4)_2\text{Ti}$ is higher by ~5 eV compared to **Ti(b)**$^+$, due to the difference in charge (the cation **Ti(b)**$^+$ is considerably more electrophilic). The HOMO for $\text{H}_2\text{C(C}_5\text{H}_4)_2\text{Ti}$ has more titanium contribution (72%) compared to **Ti(b)**$^+$, indicating that the coordination of the pendant arene in **Ti(b)**$^+$ leads to a reduced d-electron density on the metal center.

The interaction between a bent metallocene fragment and two additional ligands, e.g. Me or CO, has been explained based on MO considerations in the seminal work of Lauher and Hoffmann,[96] and a similar analysis applies for the complexes described here (Scheme S2). Analysis of the HOMO in the dicarbonyl cation **4b′** shows that the main contributions are from orbitals on the metal center (57%) and the CO ligands (22%), whereas the Cp-arene ligand is involved mainly through the arene (15%). A comparison with the HOMO composition of the neutral *ansa*-titanocene analogue $\text{H}_2\text{C(C}_5\text{H}_4)_2\text{Ti(CO)}_2$[98] shows that for **4b′**, admixture of arene orbitals comes primarily at the expense of CO contribution (Table 9).

Charge Decomposition Analysis. From the spectroscopic and structural data of the cationic dicarbonyl species **4b′** it appears that there is some degree of reduction of the arene group, resulting in Ti(IV)/dienediyl character (Scheme 4, structure **B**). Such interactions may be described by the Dewar–Chatt–Duncanson model for coordination of π-conjugated ligands to a transition metal center,[99,100] involving a combination of (i) donation from a filled ligand orbital into a empty orbital on the metal, and (ii) backdonation from an occupied metal d-orbital into an empty π^*-orbital of the ligand. Analysis of these donor–acceptor interactions was performed using the charge decomposition analysis (CDA) method of Frenking and co-workers (Table 10, see Experimental Section for details).[101,102] This partitioning scheme has been found useful in the analysis of donation and backdonation interactions in transition metal complexes. For example, the relative amount of M→CO backdonation in a series of isoelectronic hexacarbonyl complexes (from Hf(CO)$_6^{2-}$ to Ir(CO)$_6^{3+}$) was shown to correlate with the CO stretching frequencies and C–O bond distances.[103,104] Here, we use this method to evaluate the relative amount of donation/backdonation for both the arene and CO ligands in the *ansa*-Cp-arene cations described above.

For the charge decomposition routine, the complex has to be described by two separate parts (donor/acceptor). Here we take the arene moiety as the donor fragment, with the acceptor fragment consisting of the titanium atom with cyclopentadienyl and X ligands. The DFT optimized geometry of the respective *ansa*-Cp-arene cations was taken, and the cyclopentadienyl-arene ligand was split by removing the bridging atom(s) (see Scheme S2). A hydrogen atom was added to the cyclopentadienyl and arene moieties at the position of the bridge in order to obtain closed-shell fragments. The complexes thus obtained were used without further optimization to model the geometries of various

(94) Blok, A. N. J.; Budzelaar, P. H. M.; Gal, A. W. *Organometallics* **2003**, *22*, 2564.
(95) Tobisch, S.; Ziegler, T. *J. Am. Chem. Soc.* **2004**, *126*, 9059.
(96) Lauher, J. W.; Hoffmann, R. *J. Am. Chem. Soc.* **1976**, *98*, 1729.
(97) Green, J. C. *Chem. Soc. Rev.* **1998**, *27*, 263.

(98) Similar results were obtained from DV-Xα calculations on Cp$_2$Ti(CO)$_2$, see: (a) Casarin, M.; Ciliberto, E.; Gulino, A.; Fragala, I. *Organometallics* **1989**, *8*, 900.
(99) Dewar, J. S. *Bull. Soc. Chim. Fr.* **1951**, *18*, C71–C79.
(100) Chatt, J.; Duncanson, L. A. *J. Chem. Soc.* **1953**, 2939.
(101) Dapprich, S.; Frenking, G. *J. Phys. Chem.* **1995**, *99*, 9352.
(102) Frenking, G.; Pidun, U. *J. Chem. Soc., Dalton Trans.* **1997**, 1653.
(103) Szilagyi, R. K.; Frenking, G. *Organometallics* **1997**, *16*, 4807.
(104) Diefenbach, A.; Bickelhaupt, F. M.; Frenking, G. *J. Am. Chem. Soc.* **2000**, *122*, 6449.

ansa-Cp-arene coordinated titanium cations. In addition, the structures of $[Cp][\eta^6\text{-}1,3,5\text{-}Me_3C_6H_3]TiX_2^+$ (X = Me, **III″**; CO, **IV″**) were optimized for comparison, which converge to minima on the potential energy surface that have a geometry that is similar to the C_2-bridged complexes or structurally characterized analogues without bridging atom (e.g., Cp(centroid)−Ti−Ar-(centroid) angle: **III″**: 134.4°; **3c**: 130.9°; Cp′(η^6-toluene)H-fMe$_2^+$: 134°).[47,48]

The charge decomposition procedure we employed gives a measure of (fragment) molecular orbital interactions between the two closed-shell fragments as a result of complex formation, for which three terms (*d*, *b* and Δ) are obtained. Although the quantitative values obtained from the CDA scheme are not very meaningful (for instance, the values are quite sensitive to the choice of basis set),[105,106] the analysis of a series of related compounds that are calculated using the same method allows qualitative or semiquantitative trends to be extracted. Results of the charge decomposition analysis are collected in Table 10.

Table 10. Charge Decomposition Analysis of the Metal Complex−L Interaction (L = arene, (CO)$_2$)[a]

	d (e)	*b* (e)	Δ (e)	*d/b*	E_b[b]	ΔE_b[c]
			L = arene			
Ti(b)$^{3+}$	0.666	0.062	−0.005	10.7	161.3	−
Ti(c)$^{3+}$	0.669	0.040	−0.037	16.7	192.3	31.0
IIIb	0.569	0.051	−0.020	11.2	−4.3	−
IIIc	0.644	0.063	−0.038	10.2	39.2	43.5
III″	0.663	0.059	−0.046	11.2	46.6	50.9
Ti(b)$^+$	0.739	0.243	0.030	3.0	53.0	−
Ti(c)$^+$	0.788	0.256	0.007	3.1	80.2	27.2
IVb	0.782	0.182	−0.010	4.3	31.3	−
IVc	0.798	0.185	−0.029	4.3	59.7	28.4
IV″	0.771	0.168	−0.033	4.6	64.7	33.4
VIIb	0.346	0.039	−0.002	8.87	−15.1	
			L = (CO)$_2$			
IVb	0.848	0.321	0.024	2.6	65.5	
IVc	0.874	0.353	0.028	2.5	65.9	
IV″	0.877	0.379	0.026	2.3	64.9	
Cp$_2$Ti(CO)$_2$	0.918	0.476	0.012	1.93	79.4	

[a] Roman numerals correspond to the numbering scheme for the parent compounds (see Scheme S2). [b] The total bonding energy is the difference between the sum of the two fragments and the complex (kcal·mol^{-1}). [c] Relative to the analogous C$_1$-bridged compounds (**b**).

The positive values for donation (*d*) and backdonation (*b*) together with the small residual term (Δ) obtained from the charge decomposition analysis indicate that the metal−arene interaction in all compounds is properly described by the Dewar−Chatt−Duncanson model.[102] In agreement with this, the interaction of the pendant arene moiety in the d^0 titanium(IV) (**IIIb/c**) and vanadium(V) (**VIIb**) cations is dominated by the donation term *d*, and this contribution is larger for the η^6-coordinated arene in **IIIb/c** (av. ∼0.61 e) than in the case of η^1-arene coordination (**VIIb**: 0.333 e). As expected, the arene moiety becomes a stronger donor when the bridge length is increased from C$_1$ (**IIIb**: 0.569 e) to C$_2$ (**IIIc** 0.644 e). The compounds with low-valent character (Ti$^+$, **IV**) in addition show a considerable amount of charge transfer due to backdonation. Compared to the hypothetical 'naked' titanium fragments **Ti(b/c)$^+$**, the metal to arene backdonation in the dicarbonyl species **IVb/c** is reduced due to the presence of additional acceptor ligands (CO). A similar trend based on charge decomposition analysis has been observed for the metal−acetylene interaction

in M(CO)$_4$(C$_2$H$_2$) (M = Fe, Ru) and its CO dissociation product M(CO)$_3$(C$_2$H$_2$).[106]

The difference in energy between the separated fragments and the complex allows one to evaluate the total bonding energy of the interaction. Analysis of these bonding energies (E_b and ΔE_b, Table 10) shows that there is a large increase in metal−arene binding strength on going from complexes with C$_1$, *via* C$_2$, to compounds without *ansa*-bridge. The negative value for **IIIb** is puzzling at first sight, but this is likely related to the fact that the hydrogen atoms that are added after fragmentation of the ligand give rise to some steric repulsion (a similar reasoning applies for **VIIb**). For all the complexes studied, the difference in binding energy that results from changing the nature of the bridge is primarily associated with the degree of orbital overlap between the CpTiX$_2^+$ and arene fragments. The geometries of the fragments are superimposable and the energies virtually identical (within 3 kcal·mol^{-1}), whereas significantly larger differences upon interaction of the fragments are observed (Table 10).

A charge decomposition analysis was then also performed for the metal−CO interaction in the dicarbonyl species **IVb/c** and **IV″**, as well as on the neutral metallocene complex Cp$_2$Ti(CO)$_2$ (Table 10). It is clear that π-backdonation is much larger in Cp$_2$Ti(CO)$_2$ compared to the *ansa*-Cp-arene cations, in agreement with the observed differences in IR stretching frequencies (*vide supra*). Furthermore, as the *ansa*-strain is reduced on going from **IVb** to **IVc**, the value for π-backdonation to the carbonyl ligands increases. This is in line with the decrease in CO stretching frequencies in the IR spectra of **4c** compared to **4b**. These trends are readily understood based on the CDA analysis. Both the carbonyl ligands and the coordinated arene moiety compete for backdonation from the same metal d-orbital, but the backdonation to the arene is relatively invariant to the geometrical changes that result from varying the bridge length. The biggest influence of the *ansa*-bridge is seen on the electron-donating properties of the arene, which significantly increases for complexes with the longer C$_2$-bridge. This leads to a more electron-rich metal center and concomitant decrease in carbonyl stretching frequencies.

Conclusions

The compounds presented here provide experimental evidence for the versatile, multimodal coordination ability of Cp-arene ligands. Three fundamentally different arene coordination modes that are relevant to titanium-catalyzed ethylene trimerization were structurally characterized: (a) η^6-bound to a d^0 metal center (as found in calculations for nonagostic [(Cp-arene)Ti(alkyl)$_2$]$^+$ species); (b) η^1-bound to a d^0 metal center (as found in calculations for β-agostic (metallacyclic) [(Cp-arene)Ti(alkyl)$_2$]$^+$ species); (c) η^6-bound to a d^2 metal center (as found in calculations for [(Cp-arene)Ti(alkene)]$^+$ species). An interesting feature is that the latter structure was observed for the *bis*-CO-adduct, whereas calculations on the (formally isoelectronic) *bis*-ethylene adduct show an asymmetrically η^1-bound arene group. As these calculations also show that the binding of the second ethylene molecule to Ti is endergonic, with a ΔG of around 5−6 kcal mol^{-1},[25−27] it may be that the combination of an η^6-arene and two η^2-ethylenes on a cationic CpTi-moiety is too sterically demanding. This crowding could then be relieved by partial dissociation of the arene group and delocalization of the electron density of the metal by π-backdonation to the two ethylene molecules.

(105) Frenking, G.; Frohlich, N. *Chem. Rev.* **2000**, *100*, 717.
(106) Decker, S. A.; Klobukowski, M. *J. Am. Chem. Soc.* **1998**, *120*, 9342.

Increasing the length of the bridge between the cyclopentadienyl and pendant arene group has a dramatic effect on the σ-donating properties of the arene moiety, and this leads to significant differences in *hemilabile* behavior and catalysis. In addition, the electron density at the metal center is influenced. It thus appears that tuning of the ligand parameters can be used to modulate the relative energies of the Ti(II) and Ti(IV) oxidation states, and this strategy may be amendable to other early transition metals as well. The unique ability of the Cp-arene ligand to stabilize reactive, electron-deficient and/or low-valent early transition metal cations by a combination of electron-donating and -accepting properties could be more generally applicable in transition metal-mediated catalysis.

Experimental Section[107]

General Considerations. All manipulations were carried out under nitrogen atmosphere using standard glovebox, Schlenk, and vacuum-line techniques. Toluene, hexane, and pentane (Aldrich, anhydrous, 99.8%) were passed over columns of Al_2O_3 (Fluka), BASF R3-11-supported Cu oxygen scavenger, and molecular sieves (Aldrich, 4 Å). Diethyl ether and THF (Aldrich, anhydrous, 99.8%) were dried by percolation over columns of Al_2O_3 (Fluka). Cyclohexane (Labscan) was distilled from Na/K alloy, bromobenzene (Merck) from CaH_2. All solvents were degassed prior to use and stored under nitrogen. Deuterated solvents were vacuum transferred from Na/K alloy (C_6D_6 and THF-d_8, Aldrich) or from CaH_2 (C_6D_5Br, Aldrich), and stored under nitrogen. Ethylene (AGA polymer grade) was passed over BASF R3-11-supported Cu oxygen scavenger and molecular sieves (Aldrich, 4 Å). $TiCl_4$ (Fluka), MeMgCl (Aldrich, 3.0 M in THF), MeLi (Aldrich, 1.6 M in Et_2O), [PhNMe$_2$H][B(C$_6$F$_5$)$_4$] (Strem), [Ph$_3$C][B(C$_6$F$_5$)$_4$] (Strem), [R$_2$NMeH][B(C$_6$F$_5$)$_4$] (R = C$_{16}$H$_{31}$-C$_{18}$H$_{35}$, 6.2 wt % [B(C$_6$F$_5$)$_4$]$^-$ in isopar, DOW Chemicals), ^{n}BuLi (2.5 M in hexanes, Acros Organics), mesitylene (Merck), *p*-toluidine (Acros Organics), Me$_3$SiCl (Acros Organics), CO (Praxair, 4.7 LBX) and MAO (4.9 wt % Al in toluene, Akzo Nobel) were used as received. *N*,*N*,*N′*,*N′*-Tetramethylethylenediamine (TMEDA, Acros Organics) and ^{i}PrNH$_2$ (Acros Organics, dried on NaOH) were distilled before use. The compounds [Ar-CH$_2$-C$_5$H$_4$]Li (Ar = 3,5-Me$_2$C$_6$H$_3$),[108] [Ph-CMe$_2$-η^5-C$_5$H$_4$]TiCl$_3$ (**1a**),[43] [Ar-CMe$_2$-η^5-C$_5$H$_4$]TiCl$_3$ (**1b**),[44] [Ph-CMe$_2$-η^5-C$_5$H$_3$SiMe$_3$]TiCl$_3$ (**1d**),[21] [Ar-CMe$_2$-η^5-C$_5$H$_3$SiMe$_3$]TiCl$_3$ (**1f**),[55] [Ph-CMe$_2$-η^5-C$_5$H$_4$]TiMe$_3$ (**2a**),[43] [Ar-CMe$_2$-η^5-C$_5$H$_4$]TiMe$_3$ (**2b**),[44] [Ar-CMe$_2$-η^5-C$_5$H$_3$SiMe$_3$]TiMe$_3$ (**2f**),[55] V(NC$_6$H$_4$-4-Me)(N^{i}Pr$_2$)-Cl$_2$,[109] and 6,6-dimethylfulvene[110] were synthesized according to published procedures. NMR spectra were recorded on Varian VXR 300, Varian Mercury 400, or Varian Inova 500 spectrometers. The ^{1}H and ^{13}C NMR spectra were referenced internally using the residual solvent resonances and reported in ppm relative to TMS (0 ppm); *J* is reported in Hz. Assignment of NMR resonances was aided by gradient-selected COSY, NOESY, HSQC, and/or HMBC experiments using standard pulse sequences. For the various ionic compounds, NMR data for the B(C$_6$F$_5$)$_4$ anion are essentially identical and are reported only once, at the end of the Experimental Section. Elemental analyses were performed at the Microanalytical Department of the University of Groningen or Kolbe Microanalytical Laboratory (Mülheim an der Ruhr, Germany).

[Ar-CH$_2$CMe$_2$-C$_5$H$_4$]Li(TMEDA). A suspension of 15.1 g of ArCH$_2$Li(TMEDA) (62 mmol) in 200 mL of Et_2O was cooled to −20 °C. With stirring, 6,6-dimethylfulvene (7.5 mL, 62 mmol) was added dropwise. Stirring overnight at room temperature resulted

in an off-white suspension. The solvent was removed *in vacuo* and the residue washed with hexane (2 × 50 mL), giving 10.9 g of an off-white powder (44 mmol, 70%). ^{1}H NMR (400 MHz, C$_6$D$_6$/THF-d_8, 25 °C) δ 6.71 (s, 1H, Ar *p*-H), 6.66 (s, 2H, Ar *o*-H), 5.99 (ps t, 2H, Cp), 5.91 (ps t, 2H, Cp), 2.97 (s, 2H, CH2), 2.17 (s, 6H, ArMe), 1.85 (s, 12H, TMEDA), 1.82 (s, 4H, TMEDA), 1.37 (s, 6H, CMe$_2$).

General Procedure for the Synthesis of Ar-Z-C$_5$H$_3$(SiMe$_3$)$_2$. To a cold (−10 °C) suspension of [Ar-Z-C$_5$H$_4$]Li in Et_2O/THF (~1:1) was added an excess of Me$_3$SiCl, which was subsequently stirred overnight at room temperature. After removal of volatiles, the product was extracted into Et_2O, and 1.05 equiv of BuLi was added at 0 °C. The mixture was stirred overnight at room temperature, and some THF was added to dissolve all precipitation. Cooling to 0 °C and addition of excess Me$_3$SiCl gave a turbid reaction mixture. After stirring overnight at room temperature, the solvent was pumped off and the yellow oily product separated from LiCl by dissolving it in CH_2Cl_2 with subsequent filtration. Attempted aqueous workup as described for the synthesis of mono(trimethylsilyl)-substituted cyclopentadienes[43] resulted in hydrolysis of one of the SiMe$_3$ groups, and therefore the solutions of crude product were used without further purification.

[Ar-CH$_2$CMe$_2$-η^5-C$_5$H$_4$]TiCl$_3$ (1c). A solution of [Ar-CH$_2$CMe$_2$-C$_5$H$_4$]Li(TMEDA) (1.34 g, 3.85 mmol) in 40 mL of Et_2O/THF (1:1) was stirred at 0 °C. To this was added 5 mL of SiMe$_3$Cl (~10 equiv), and the resulting mixture was allowed to warm to room temperature and stirred overnight. After addition of 50 mL of water, the yellow product was extracted into light petroleum ether. Kugelrohr distillation afforded 0.845 g (2.83 mmol, 74%) of Ar-CH$_2$CMe$_2$-C$_5$H$_4$SiMe$_3$ as a yellow oil, which was added to a stirred solution of $TiCl_4$ (0.311 mL, 2.84 mmol) in 25 mL of CH_2Cl_2 at −60 °C. The mixture was slowly warmed to room temperature and stirred overnight, after which all volatiles were removed. To remove residual CH_2Cl_2, the brownish residue was stirred with 10 mL of pentane, which was subsequently pumped off. Extraction of the product into hexane and cooling the extract to −80 °C overnight gave **1c** as brown/orange powder (0.50 g, 1.32 mmol, 46% based on $TiCl_4$) ^{1}H NMR (500 MHz, C$_6$D$_6$, 25 °C) δ 6.70 (s, 1H, Ar *p*-H), 6.18 (s, 2H, Ar *o*-H), 6.12 (ps t, *J* = 2.6, 2H, Cp), 6.01 (ps t, *J* = 2.6, 2H, Cp), 2.39 (s, 2H, CH$_2$), 2.08 (s, 6H, Ar Me), 1.20 (s, 6H, CMe$_2$). ^{13}C NMR (125.7 MHz, C$_6$D$_6$, 25 °C) δ 153.90 (Cp *ipso*-C), 137.06 (Ar *m*-C), 137.02 (Ar *ipso*-C), 128.78 (Ar *o*-CH), 128.41 (Ar *p*-CH), 123.18 (Cp CH), 121.59 (Cp CH), 51.64 (CH$_2$), 38.48 (*C*Me$_2$), 26.78 (C*Me*$_2$), 21.22 (Ar Me).

[Ar-CH$_2$CMe$_2$-η^5-C$_5$H$_4$]TiMe$_3$ (2c). To a solution of **1c** (307 mg, 0.809 mmol) in 25 mL of Et_2O at −30 °C was added 0.89 mL of MeMgCl (3.0 M solution in THF, 2.67 mmol). The mixture was stirred for 2 h while slowly warming to room temperature. All volatiles were removed *in vacuo*. To remove residual Et_2O, the product was stirred with 10 mL of pentane, which was subsequently pumped off. Extraction with pentane (2 × 20 mL) and cooling the extracts to −80 °C gave 155 mg of light green powder. Further concentration of the mother liquor and cooling to −80 °C afforded another 53 mg of **2c**. Total yield: 203 mg (0.638 mmol, 79%). ^{1}H NMR (500 MHz, C$_6$D$_6$, 25 °C) δ 6.77 (s, 1H, Ar *p*-H), 6.52 (s, 2H, Ar *o*-H), 5.80 (m, 4H, Cp), 2.62 (s, 2H, CH$_2$), 2.18 (s, 6H, Ar Me), 1.31 (s, 9H, Ti Me), 1.04 (s, 6H, CMe$_2$). ^{13}C NMR (125.7 MHz, C$_6$D$_6$, 25 °C) δ 143.89 (Cp *ipso*-C), 138.32 (Ar *ipso*-C), 136.80 (Ar *m*-C), 129.07 (Ar *o*-C), 128.09 (Ar *p*-CH), 113.72 (Cp CH), 109.40 (Cp CH), 62.78 (TiMe), 52.45 (CH$_2$), 36.93 (*C*Me$_2$), 27.24 (C*Me*$_2$), 21.37 (Ar Me). Anal. Calcd for C$_{20}$H$_{30}$Ti: C, 75.46; H, 9.50. Found: C, 75.2; H, 9.68.

{[η^6-Ar-CH$_2$CMe$_2$-η^5-C$_5$H$_4$]TiMe$_2$}[B(C$_6$F$_5$)$_4$] (3c). A solution of **2c** (49 mg, 154 μmol) in 0.5 mL of C$_6$H$_5$Br was cooled to −30 °C. A cold solution of [Ph$_3$C][B(C$_6$F$_5$)$_4$] (135 mg, 146 μmol) in bromobenzene ((~0.5 mL) was layered on top of this. Slow diffusion at −30 °C resulted in a dark orange oil, which solidified in the course of a couple of days. Washing with pentane and drying *in vacuo* gave **3c** as orange needles. Yield: 138 mg (140 μmol,

(107) Representative complexes only. Full details provided in the Supporting Information.
(108) Licht, E. H.; Alt, H. G.; Karim, M. M. *J. Organomet. Chem.* **2000**, *599*, 275.
(109) Bouwkamp, M. W.; Batinas, A. A.; Witte, P. T.; Hubregtse, T.; Dam, J.; Meetsma, A.; Teuben, J. H.; Hessen, B. *Organometallics* **2008**, *27*, 4071.
(110) Stone, K. J.; Little, R. D. *J. Org. Chem.* **1984**, *49*, 1849.

96%). ^{1}H NMR (500 MHz, C$_6$D$_5$Br, −25 °C) δ 7.15 (s, 1H, Ar *p*-H), 6.62 (s, 2H, Cp), 6.04 (s, 2H, Ar *o*-H), 5.48 (s, 2H, Cp), 2.10 (s, 2H, CH$_2$), 2.07 (s, 6H, Ar Me), 0.87 (s, 6H, CMe$_2$), 0.07 (s, 6H, Ti Me). ^{13}C NMR (125.7 MHz, C$_6$D$_5$Br, −25 °C) δ 149.0 (s, Ar *m*-C), 143.1 (s, Ar *ipso*-C), 140.8 (s, Cp *ipso*-C), 133.7 (d, *J* = 169, Ar *p*-CH), 126.5 (overlapped, Ar *o*-CH), 122.9 (d, overlapped, Cp CH), 113.1 (d, *J* = 174, Cp CH), 68.5 (q, *J* = 127, Ti Me), 48.1 (t, *J* = 131, CH$_2$), 39.8 (s, *C*Me$_2$), 30.2 (C*Me*$_2$), 22.0 (q, *J* = 129, Ar Me). Anal. Calcd for C$_{43}$H$_{27}$BF$_{20}$Ti: C, 52.57; H, 2.77; Ti, 4.88. Found: C, 52.38; H, 2.86; Ti, 4.88.

General procedure for NMR-tube scale synthesis of ionic compounds 3d−h. A solution of the appropriate neutral trimethyl complex (∼8 mg) in 0.4 mL of C$_6$D$_5$Br was prepared in the glovebox and cooled to −30 °C. To this was added 1.05 equiv of [Ph$_3$C][B(C$_6$F$_5$)$_4$], resulting in immediate color change to dark red. The cold NMR tube was taken out of the glovebox immediately and frozen in liquid N$_2$. Alternatively, for reactions in CD$_2$Cl$_2$, the solvent was vacuum-transferred at −196 °C into an NMR tube containing a mixture of the solid starting materials, which was then closed and allowed to thaw at −60 °C. The cold solutions were inserted in the precooled probe of the NMR spectrometer and analyzed by 1D and 2D experiments, which indicated full conversion to the ionic species with concomitant formation of Ph$_3$CMe.

{[η^6-Ph-CMe$_2$-η^5-C$_5$H$_3$SiMe$_3$]TiMe$_2$}[B(C$_6$F$_5$)$_4$] (3d). ^{1}H NMR (500 MHz, C$_6$D$_5$Br, −30 °C) δ 7.58 (br, 3H, Ph), 6.91 (s, 1H, Cp), 6.08 (s, 2H, Ph), 5.63 (s, 1H, Cp), 5.32 (s, 1H, Cp), 1.02 (s, 6H, CMe$_2$), 0.71 (br, 3H, TiMe), 0.66 (br, 3H, TiMe), 0.12 (s, 9H, SiMe$_3$). ^{13}C NMR (125.7 MHz, C$_6$D$_5$Br, −30 °C) δ 138.1 (Cp*C*SiMe$_3$), 132.9 (Ar *ipso*-C), 131.2 (Cp CH), 128.4 (Ph CH), 124.6 (Cp *ipso*-C + Ph *o*-CH), 118.3 (Cp CH), 117.5 (Cp CH), 69.9 (TiMe), 40.6 (*C*Me$_2$), 21.5 (C*Me*$_2$), −1.2 (SiMe$_3$).

{[η^6-Ar-CMe$_2$-η^5-C$_5$H$_4$]Ti(CO)$_2$}[B(C$_6$F$_5$)$_4$] (4b). A powdered sample of solid **3b** (103 mg, 106 μmol) was exposed to 1 bar of CO. After standing at room temperature for 3 days, the orange color of the starting material had darkened to red-brown. The excess CO was pumped off and the residue washed with 5 mL of cold (−30 °C) bromobenzene. Subsequent washing with pentane and drying *in vacuo* gave 87 mg of **4b** as a red powder (87.5 μmol, 82%). Crystals suitable for X-ray analysis were obtained by diffusion of cyclohexane into a bromobenzene solution of **4b**. ^{1}H NMR (500 MHz, C$_6$D$_5$Br, 25 °C) δ 5.00 (s, 1H, Ar *p*-H), 4.95 (s, 2H, Cp), 4.38 (s, 2H, Ar *o*-H), 3.91 (s, 2H, Cp), 1.69 (s, 6H, Ar Me), 0.69 (s, 6H, CMe$_2$). ^{13}C NMR for the cationic part (125.7 MHz, C$_6$D$_5$Br, 25 °C) δ 227.3 (s, CO), 136.4 (s, Ar *m*-C), 104.8 (d, *J* = 180, Cp CH), 102.6 (d, *J* = 173, Ar *o*-CH), 100.3 (d, *J* = 175, Ar *p*-CH), 91.3 (s, Cp *ipso*-C), 86.8 (s, Ar *ipso*-C), 83.4 (d, *J* = 181, Cp CH), 38.7 (s, *C*Me$_2$), 21.3 (q, *J* = 129, Ar Me), 19.5 (q, *J* = 127, C*Me*$_2$). IR (ν, cm^{-1}), film from C$_6$D$_5$Br on KBr plates: 2055, 2022 (CO); nujol mull: 2052, 2023 (CO). Anal. Calcd for C$_{42}$H$_{19}$BF$_{20}$O$_2$Ti: C, 50.74; H, 1.93. Found: C, 50.58; H, 2.00.

Identification of Acetone As a Product from the Reaction of 3b with CO. An NMR tube containing solid **3b** was degassed on a high-vacuum line and backfilled with 1 bar of CO. After standing at room temperature for 4 days, the color of the solid had turned reddish. The tube was frozen in liquid N$_2$, the valve opened under N$_2$ flow, and 0.5 mL of wet C$_6$D$_5$Br was added with a pipet. The tube was closed and allowed to warm to room temperature. The ^{1}H NMR spectrum showed signals for **4b**, a broad signal attributed to H$_2$O, and acetone (δ 1.81 ppm). The peaks for **4b** slowly disappeared in the course of several hours. In a control experiment, a dried (empty) tube was frozen in liquid N$_2$, and under N$_2$ flow 0.5 mL of wet C$_6$D$_5$Br was added. ^{1}H NMR spectroscopy showed only residual solvent peaks and some H$_2$O, showing that the acetone observed is not due to adventitious traces, but stems from the reaction.

General Procedure for NMR Tube Scale Carbonylation of 3a−f,h. A C$_6$D$_5$Br solution of the appropriate titanium dimethyl cation (**3a−f** or **3h**), either isolated or prepared *in situ* from **2a−f** or **2h** and [Ph$_3$C][B(C$_6$F$_5$)$_4$], was degassed on a high-vacuum line

by three freeze−pump−thaw cycles. The tube was backfilled with 1 bar of CO, and the reaction was monitored by ^{1}H NMR. When all starting material was consumed (<30 min for compounds with C$_1$ bridge, several hours for C$_2$-bridged compounds), the excess CO was pumped off. Samples for IR spectroscopy were prepared in the glovebox. A drop of the solution was taken from the NMR tube and placed on top of a KBr plate. The solvent was pumped off, leaving a red film on the plate, which was placed immediately in the FTIR spectrometer in the glovebox, and the IR spectrum was recorded.

{[η^6-Ar-CH$_2$CMe$_2$-η^5-C$_5$H$_4$]Ti(CO)$_2$}[B(C$_6$F$_5$)$_4$] (4c). ^{1}H NMR (500 MHz, C$_6$D$_5$Br, 25 °C) δ 5.37 (s, 2H, Ar *o*-H), 5.15 (s, 2H, Cp), 4.78 (s, 2H, Cp), 4.62 (s, 1H, Ar *p*-H), 2.15 (s, 2H, CH$_2$), 1.72 (s, 6H, ArMe), 0.87 (s, 6H, CMe$_2$). ^{13}C NMR for the cationic part (125.7 MHz, C$_6$D$_5$Br, 25 °C) δ 237.0 (CO), 137.0 (Cp *ipso*-C), 129.0 (Ar *m*-C), 128.4 (Ar *ipso*-C), 110.3 (Ar *o*-CH), 105.0 (Ar *p*-CH), 97.1 (Cp CH), 93.3 (Cp CH), 50.8 (CH$_2$), 39.4 (*C*Me$_2$), 30.0 (C*Me*$_2$), 21.0 (ArMe). IR (ν, cm^{-1}), film from C$_6$D$_5$Br on KBr plates: 2039, 1997 (CO).

[Ar-CMe$_2$-η^5-C$_5$H$_4$]VCl(N^{i}Pr$_2$)(NC$_6$H$_4$-4-Me) (5b). Onto a mixture of 0.20 g (0.64 mmol) of V(NC$_6$H$_4$-4-Me)(N^{i}Pr$_2$)Cl$_2$ and 0.14 g (0.64 mmol) of [Ar-CMe$_2$-C$_5$H$_4$]Li, 10 mL of THF was condensed at liquid nitrogen temperature. The mixture was warmed to room temperature and stirred overnight. The solvent was removed *in vacuo*, and residual THF was removed by stirring the red residue with 5 mL of pentane, which was subsequently pumped off. Extraction with 10 mL of pentane and cooling to −25 °C yielded 0.20 g of **5b** as red crystals (0.40 mmol, 65%). ^{1}H NMR (400 MHz, C$_6$D$_6$, 25 °C) δ 7.19 (d, *J* = 8.2, 2H, *p*-tolyl H), 6.97 (s, 2H, Ar *o*-H), 6.76 (d, *J* = 8.2, 2H, *p*-tolyl H), 6.65 (s, 1H, Ar *p*-H), 6.32 (s, 1H, Cp), 5.91 (s, 1H, Cp), 5.79 (s, 1H, Cp), 5.51 (s, 1H, Cp), 5.01 (sept, *J* = 6.3, 1H, ^{i}Pr CH), 3.34 (sept, *J* = 6.3, 1H, ^{i}Pr CH), 2.10 (s, 6H, ArMe), 2.0 (s, 3H, *p*-tolyl Me), 1.98 (s, 3 H, CMe$_2$), 1.79 (d, *J* = 6.3, 3H, ^{i}Pr Me), 1.73 (s, 3H, *p*-tolyl Me), 1.28 (d, *J* = 6.3, 3H, ^{i}Pr Me), 1.04 (d, *J* = 6.3, 3H, ^{i}Pr Me), 0.75 (d, *J* = 6.3, 3H, ^{i}Pr Me). ^{13}C NMR (100 MHz, C$_6$D$_6$, 25 °C) δ 151.7 (Cp *ipso*-C), 137.6 (Ar *ipso*-C), 137.3 (Ar *m*-C), 135.9 (*p*-tolyl *p*-C), 129.2 (*p*-tolyl CH), 127.6 (Ar *p*-CH), 125.6 (*p*-tolyl CH), 124.3 (Ar *o*-CH), 113.7 (Cp CH), 108.0 (Cp CH), 106.3 (Cp CH), 100.9 (Cp CH), 65.4 (^{i}Pr CH), 59.1 (^{i}Pr CH), 41.3 (*C*Me$_2$), 31.1 (^{i}Pr Me), 29.7 (C*Me*$_2$), 29.6 (C*Me*$_2$), 27.3 (^{i}Pr Me), 21.6 (ArMe) 21.2 (*p*-tolyl Me), 19.3 (^{i}Pr Me), 17.4 (^{i}Pr Me), *p*-tolyl *ipso*-C not located. Anal. Calcd (%) for C$_{29}$H$_{40}$N$_2$VCl: C, 69.24; H, 8.01; N, 5.57. Found: C, 69.20; H, 8.06; N, 5.64.

[Ar-CMe$_2$-η^5-C$_5$H$_4$]VMe(N^{i}Pr$_2$)(NC$_6$H$_4$-4-Me) (6b). To a solution of 1.08 g (2.15 mmol) of **5b** in 30 mL of Et$_2$O at −40 °C was added 1.36 mL (2.15 mmol) of MeLi (1.58 M in Et$_2$O). The mixture was stirred at −40 °C for 1.5 h and then slowly warmed up to −10 °C. The solvent was removed *in vacuo* at this temperature, and the residue was stirred with 5 mL of cold pentane, which was subsequently pumped off. Extraction with 20 mL of cold (−10 °C) pentane, followed by cooling to −80 °C yielded **6b** as red crystals (0.65 g, 1.35 mmol, 69%). ^{1}H NMR (400 MHz, C$_6$D$_6$, 25 °C) δ 7.19 (d, *J* = 8.1, 2H, *p*-tolyl H), 6.96 (s, 2H, Ar *o*-H), 6.87 (d, *J* = 8.1, 2H, *p*-tolyl H), 6.65 (s, 1H, Ar *p*-H), 5.78 (m, 1H, Cp), 5.69 (m, 1H, Cp), 5.64 (m, 1H, Cp), 5.56 (m, 1H, Cp), 4.48 (sept, *J* = 6.3, 1H, ^{i}Pr CH), 3.29 (sept, *J* = 6.3, 1H, ^{i}Pr CH), 2.11 (s, 6H, ArMe), 2.08 (s, 3H, *p*-tolyl Me), 1.72 (d, *J* = 6.3, 3H, ^{i}Pr Me), 1.67 (d, *J* = 6.3, 3H, ^{i}Pr Me), 1.64 (s, 3 H, CMe$_2$), 1.61 (s, 3 H, CMe$_2$), 0.84 (2 × d, *J* = 6.3, total 6H, ^{i}Pr Me), 0.82 (br s, 3H, VMe). ^{13}C NMR (100 MHz, C$_6$D$_6$, 25 °C) δ 151.4 (Cp *ipso*-C), 137.3 (Ar *m*-C), 133.5 (Ar *ipso*-C), 132.1 (*p*-tolyl *p*-C), 129.2 (*p*-tolyl CH), 127.6 (Ar *p*-CH), 125.8 (*p*-tolyl CH), 124.2 (Ar *o*-CH), 111.7 (Cp CH), 106.2 (Cp CH), 105.3 (Cp CH), 103.9 (Cp CH), 62.7 (^{i}Pr CH), 55.2 (^{i}Pr CH), 39.3 (*C*Me$_2$), 32.5 (^{i}Pr Me), 31.0 (C*Me*$_2$) 30.8 (C*Me*$_2$), 27.2 (^{i}Pr Me), 21.6 (ArMe), 21.1 (*p*-tolyl Me), 20.8 (^{i}Pr Me), 19.0 (^{i}Pr Me). VMe, Ar *ipso*-C and *p*-tolyl *ipso*-C not observed. Anal. Calcd (%) for C$_{30}$H$_{43}$N$_2$V: C, 74.66; H, 8.98; N, 5.80. Found: C, 74.6; H, 9.15; N, 5.65.

{[η^1-Ar-CMe$_2$-η^5-C$_5$H$_4$]V(N^{i}Pr$_2$)(NC$_6$H$_4$-4-Me)}[B(C$_6$F$_5$)$_4$] (7b).
To a solution of 29 mg (60 μmol) of **6b** in 1 mL of dichloromethane was added a solution of [Ph$_3$C][B(C$_6$F$_5$)$_4$] (55 mg, 60 μmol) in 1 mL dichloromethane. The resulting dark-red solution was shaken for 5 min, after which cyclohexane (~5 mL) was layered on top of the dichloromethane solution. After slow diffusion overnight at room temperature, crystalline material precipitated. The supernatant was decanted, and the crystals were dried *in vacuo* to give 66 mg (57 μmol, 95%) of **7b**. ^{1}H NMR (500 MHz, CD$_2$Cl$_2$, 0 °C) δ 7.29 (d, J = 7.8, 2H, *p*-tolyl), 7.21 (d, J = 7.8, 2H, *p*-tolyl), 7.07 (s, 1H, Ar *p*-H), 6.99 (s, 1H, Ar *o*-H), 6.02 (s, 1H, Cp), 5.97 (s, 1H, Cp), 5.95 (s, 1H, Cp), 5.70 (s, 1H, Cp), 5.22 (s, 1H, Ar *o*-H), 3.64 (sept, J = 6.34, 1H, ^{i}Pr CH), 3.57 (sept, J = 6.3, 1H, ^{i}Pr CH), 2.51 (s, 3H, ArMe), 2.45 (s, 3H, ArMe), 2.44 (s, 3H, *p*-tolyl Me), 1.93 (s, 3 H, CMe$_2$), 1.86 (d, J = 6.3, 3H, ^{i}Pr Me), 1.53 (s, 3 H, CMe$_2$), 1.23 (d, J = 6.3, 3H, ^{i}Pr Me), 0.97 (d, J = 6.3, 3H, ^{i}Pr Me), 0.54 (d, J = 6.3, 3H, ^{i}Pr Me). ^{13}C NMR for the cationic part (125.7 MHz, CD$_2$Cl$_2$, −10 °C) δ 157.5 (s, Ar *m*-C), 156.5 (s, Ar *m*-C), 148.4 (s, Ar *ipso*-C), 139.9 (s, *p*-tolyl *p*-C), 131.2 (d, J = 161, Ar *p*-CH), 129.9 (d, J = 160, *p*-tolyl CH), 127.4 (s, Cp *ipso*-C), 125.7 (d, J = 162, *p*-tolyl CH), 119.0 (d, J = 161, Ar *o*-CH), 109.8 (d, J = 179, Cp CH), 109.2 (d, J = 180, Cp CH), 106.5 (d, J = 175, Cp CH), 100.2 (d, J = 176, Cp CH), 93.8 (d, J = 146, Ar *o*-CH), 67.7 (d, J = 138, ^{i}Pr CH), 60.3 (d, J = 135, ^{i}Pr CH), 38.0 (s, *C*Me$_2$), 33.0 (q, J = 127, ^{i}Pr Me), 27.3 (q, J = 128, C*Me*$_2$), 26.4 (q, J = 127, ^{i}Pr Me), 24.6 (q, J = 127, C*Me*$_2$), 23.3 (q, J = 128, ArMe), 23.0 (q, J = 128, ArMe), 21.4 (q, J = 127, *p*-tolyl Me), 20.6 (q, J = 128, ^{i}Pr Me), 18.7 (q, J = 127, ^{i}Pr Me). *p*-tolyl *ipso*-C not located. Anal. Calcd for C$_{53}$H$_{40}$N$_2$VBF$_{20}$: C, 55.52; H, 3.52; N, 2.44. Found: C, 54.10 [Due to limited thermal stability of the compound, carbon values were found to be low for several attempts.]; H, 3.69; N, 2.25.

NMR data for the [B(C$_6$F$_5$)$_4$] anion. ^{13}C NMR (125.7 MHz, C$_6$D$_5$Br, −25 °C) δ 149.02 (d, J_{CF} = 242.9, *o*-CF), 138.92 (d, J_{CF} = 237.4, *p*-CF), 137.02 (d, J_{CF} = 239.9, *m*-CF), 124.30 (br, C$_6$F$_5$ *ipso*-C). ^{19}F NMR (470 MHz, C$_6$D$_5$Br, −25 °C) δ −132.9 (*o*-F), −162.5 (*p*-F), −166.4 (*m*-F).

General Procedure for Trimerization Experiments. In the glovebox, (pre)catalyst stock solutions were made (**1**: 50 mol; μmol; **2**: 30 μmol) in 10 mL of toluene and stored at −30 °C. From these solutions, 1.0 mL portions were used for trimerization experiments. All trimerization runs were performed in a 1.0 L stainless steel autoclave, predried under reduced pressure, charged with 200 mL of dry toluene, equilibrated at 30 °C, and pressurized with 10 bar of ethene. For the runs with trichlorides **1**, 250 equiv of MAO were injected first into the autoclave (using a pneumatically operated injector). In the glovebox, the catalyst solution was mixed with 250 equiv of MAO and rapidly (within 1 min after mixing) injected into the autoclave (total Al/Ti ratio = 500). For the runs with **2**, 1.05 equiv of [R$_2$NMeH][B(C$_6$F$_5$)$_4$] (R = C$_{16}$H$_{31}$-C$_{18}$H$_{35}$, 6.2 wt % B(C$_6$F$_5$)$_4$$^-$ in Isopar, DOW Chemicals) mixed with ~40 mg of MAO as scavenger, were injected first. The reaction was started by injecting the solution of the titanium trialkyl (**2**). The ethylene pressure was kept constant during the reaction by replenishing flow. The reactor was stirred for 15 min, a known amount of cyclohexane was injected, after which a sample of the liquids was taken for GC analysis. The reactor was vented, the polymeric material collected, washed with acidified ethanol and dried in a vacuum oven at 80 °C. Integration of the cyclohexane and 1-hexene peaks in the GC from the liquid samples gives the amount of 1-hexene that is produced.

Computational Studies. Calculations were performed with the *Gaussian03* program using density functional theory (DFT).[111a] Geometries of the cations **3b/c**, **4b/c**, and **7b** were fully optimized starting from the X-ray structures using the B3LYP exchange-correlation functional with the LANL2DZ basis set on the metal center, and 6-311G(d) basis sets on all other atoms. The anions were omitted in the calculations. Optimizations were performed without (symmetry) constraints, and the resulting structures were

confirmed to be minima on the potential energy surface by frequency calculations (number of imaginary frequencies = 0). The frequency analysis of **7b** was performed using *Gaussian03W*.[111b] Charge decomposition analysis was performed using the CDA program by Dapprich and Frenking.[112] The input for the CDA program was generated from single point calculations on the appropriate species (without bridging atoms, as described in the main text) with double-ζ basis sets used throughout (LANL2DZ on the metal, 6-31G(d) on all nonmetal atoms). Geometry optimization of **3b** using double-ζ basis sets on all atoms resulted in a structure with metrical parameters that are virtually identical to the ones obtained using 6-311G(d) on the nonmetal atoms. For visualization of the computed structures and molecular orbitals the program *MOLEKEL* 4.3 was used.[113]

X-ray Crystal Structures. Suitable crystals of **3a**−**3c**, **3f**, **4b**, and **6b** were mounted on top of a glass fiber in a drybox and transferred, using inert-atmosphere handling techniques, into the cold nitrogen stream of a Bruker SMART APEX CCD diffractometer. The final unit cell was obtained from the *xyz* centroids of 9603 (**3a**), 6331 (**3b**), 3130 (**3c**), 4369 (**3f**), 8874 (**4b**), or 5280 (**7b**) reflections after integration. Intensity data were corrected for Lorentz and polarization effects, scale variation, for decay and absorption: a multiscan absorption correction was applied, based on the intensities of symmetry-related reflections measured at different angular settings (*SADABS*).[114] The structures were solved by Patterson methods and extension of the model was accomplished by direct methods applied to difference structure factors using the program *DIRDIF*.[115] A difference Fourier synthesis resulted in the location of all hydrogen atoms for **3b**, **3f**, **4b** and **7b** and the hydrogen atom coordinates and isotropic displacement parameters were refined freely. For **3a** and **3c**, the hydrogen atoms were generated by geometrical considerations, constrained to idealized geometries, and allowed to ride on their carrier atoms with an isotropic displacement parameter related to the equivalent displacement parameter of their carrier atoms. The crystals obtained for **3a** and **3c** showed weak scattering power. For **3a**, from the solution it was clear the bromobenzene solvate molecule was highly disordered over an inversion center: no satisfactory discrete model could be fitted in this density. The *BYPASS* (*SQUEEZE*) procedure[116] was used to take into account the electron density in the potential solvent area of 570.4 Å^3/unit cell. In addition, refinement was complicated by a disorder in the cyclopentadienyl and phenyl positions, which appeared to be interchangeable. Possibly, the similarity of the C$_5$ and C$_6$ rings results in nonpreferential packing. The disorder results in unrealistic displacement parameters when allowed to vary anisotropically, and the structure is so poorly defined that it only serves to establish connectivities. To improve the parameters to chemically more reasonable values, ultimately restrain instructions (DELU, SIMU) for the C atoms were applied in the refinement. For **3c**, two atoms, C(319) and (C44), showed unrealistic displacement parameters when allowed to vary anisotropically, suggesting dynamic disorder, and restrain instructions were applied in the refinement to obtain reasonable parameters. For **4b**, the final difference Fourier map revealed features within the range −1.01 to +0.60(8) e/Å^3 located near the Br position of the bromobenzene

(111) (a) Frisch, M. J.; et al. *Gaussian 03*, Revision B.05; Gaussian, Inc.: Wallingford CT, 2004. (b) Frisch, M. J.; et al. *Gaussian 03*, Revision C.02; Gaussian, Inc.: Wallingford CT, 2004.

(112) Dapprich, S.; Frenking, G. *CDA 2.1*; Philipps-Universität Marburg: Marburg, 1995. Available at http://www.uni-marburg.de/fb15/ag-frenking/cda.

(113) Flükiger, P.; Lüthi, H. P.; Portmann, S.; Weber, J. *MOLEKEL 4.0*; Swiss National Supercomputing Centre, CSCS: Manno (Switzerland), 2000.

(114) Sheldrick, G. M., *SADABS, Version 2.10*, Multi-Scan Absorption Correction Program; University of Göttingen: Germany, 2006.

(115) Beurskens, P. T.; Beurskens, G.; De Gelder, R.; García-Granda, S.; Gould, R. O.; Israël, R.; and Smits, J. M. M. *The DIRDIF-99 Program System*; Crystallography Laboratory, University of Nijmegen: The Netherlands, 1999.

(116) Van der Sluis, P.; Spek, A. L. *Acta Crystallogr. A* **1990**, *46*, 194.

Table 11. Crystallographic Data for **3a**–**3c** and **3f**

	3a	3b	3c	3f
chemical formula	$[C_{16}H_{21}Ti]^+$ $[C_{24}BF_{20}]^-$·0.5(C_6H_5Br)	$[C_{18}H_{25}Ti]^+$ $[C_{24}BF_{20}]^-$	$[C_{19}H_{27}Ti]^+$ $[C_{24}BF_{20}]^-$	$[C_{21}H_{33}SiTi]^+$ $[C_{24}BF_{20}]^-$
M_r	1018.77	968.31	982.33	1040.49
crystal system	monoclinic	monoclinic	monoclinic	triclinic
color, habit	orange, platelet	orange, block	orange, needle	orange, block
size (mm^3)	0.47 × 0.13 × 0.06	0.37 × 0.17 × 0.14	0.55 × 0.10 × 0.08	0.31 × 0.15 × 0.12
space group	$P2_1/c$	$P2_1/c$	$P2_1/n$	$P\bar{1}$
a (Å)	10.791(1)	12.0159(9)	14.173(3)	9.6470(8)
b (Å)	13.320(1)	19.541(1)	18.378(3)	12.960(1)
c (Å)	28.398(3)	15.977(1)	29.769(5)	17.683(2)
α (deg)	−	−	−	102.781(1)
β (deg)	91.066(2)	91.830(1)	97.089(4)	90.754(2)
γ (deg)	−	−	−	96.832(2)
V (Å^3)	4081.1(7)	3749.5(4)	7695(2)	2139.0(3)
Z	4	4	8	2
ρ_{calc}, g·cm^{-3}	1.658	1.715	1.696	1.615
μ(Mo Kα), cm^{-1}	3.3	3.62	3.54	3.5
$F(000)$	2024	1936	3936	1048
temp (K)	100(1)	100(1)	100(1)	100(1)
θ range (deg)	2.39−25.03	2.19−27.55	2.32−25.35	2.48−26.02
data collected (h,k,l)	−12:12, −15:15, −33:33	−13:14, −23:23, −19:19	−17:17, −22:22, −35:35	−11:11, 15:15, −21:20
min and max transm	0.8189, 0.9822	0.8689, 0.9510	0.7932, 0.9722	0.8471, 0.9592
no. of rflns collected	28595	26584	55823	16765
no. of indpndt reflns	7155	6618	14058	8230
observed reflns ($F_o \geq 4.0\sigma(F_o)$)	4302	4283	6809	5380
R(F) (%)	7.07	5.05	6.36	5.59
wR(F^2) (%)	19.16	11.81	14.49	13.11
GooF	1.041	1.021	0.950	1.026
weighting a,b	0.1, 0.0	0.0495, 0.6185	0.0510, 0.0	0.0558, 0.0670
params refined	563	677	1183	745
min, max resid dens	−0.4, 1.1(1)	−0.55, 0.34(7)	−0.49, 0.42(8)	−0.40, 0.91(8)

Table 12. Crystallographic Data for **4b** and **7b**

	4b	7b
chemical formula	$[C_{18}H_{19}O_2Ti]^+[C_{24}BF_{20}]^-$· C_6H_5Br	$[C_{29}H_{40}N_2V]^+[C_{24}BF_{20}]^-$
M_r	1151.27	1146.63
crystal system	monoclinic	monoclinic
color, habit	red, needle	red, platelet
size (mm^3)	0.51 × 0.19 × 0.11	0.47 × 0.28 × 0.19
space group	$P2_1/c$	$P2_1/n$
a (Å)	15.902(2)	15.858(2)
b (Å)	17.780(2)	15.996(2)
c (Å)	17.100(2)	20.876(2)
α (deg)	−	−
β (deg)	115.144(2)	104.360(2)
γ (deg)	−	−
V (Å^3)	4376.7(9)	5130.1(10)
Z	4	4
ρ_{calc}, g·cm^{-3}	1.747	1.485
μ(Mo Kα), cm^{-1}	12.36	3.05
$F(000)$	2280	2320
temp (K)	100(1)	100(1)
θ range (deg)	2.57−25.68	2.47−26.73
data collected (h,k,l)	−19:19, −21:21, −20:20	−20:20, −20:20, −25:26
min and max transm	0.6196, 0.8760	0.8465, 0.9437
no. of rflns collected	32715	41370
no. of indpndt reflns	8296	10849
observed reflns	5883 ($F_o \geq 4\sigma(F_o)$)	8324 ($F_o \geq 4\sigma(F_o)$)
R(F) (%)	4.95	4.32
wR(F^2) (%)	12.61	11.06
GooF	1.036	1.026
weighting a,b	0.0579, 3.5774	0.0588, 0.9039
params refined	754	854
min, max resid dens	−1.01, 0.60(8)	−0.32, 0.42(6)

dichloromethane solvate molecule was highly disordered. No satisfactory discrete model could be fitted in this density. The *BYPASS* (*SQUEEZE*) procedure[116] was used to take into account the electron density in the potential solvent accessible area (348.5 Å^3/unit cell). All refinement and geometry calculations were performed with the program packages *SHELXL*[117] and *PLATON*.[118] Crystal data and details on data collection and refinement are presented in Tables 11 and 12.

Supporting Information Available: Full experimental section, crystallographic data (CIF format) for **3a**−**c**, **3f**, **4b**, and **7b**, Cartesian coordinates of DFT optimized structures (**3b′**, **3c′**, **4b′**, **4c′**, and **7b′**), frontier molecular orbital representations, representations of the orbitals involved in donation/backdonation according to CDA, details of the EXSY analysis for **7b/c**, and full citation for Gaussian03 (ref 111). This material is available free of charge via the Internet at http://pubs.acs.org.

JA810089F

solvate molecule. For **7b**, refinement was complicated by a disorder problem: from the solution it was clear that the position of a

(117) Sheldrick, G. M. *SHELXL-97*, Program for the Refinement of Crystal Structures; University of Göttingen: Germany, 1997.

(118) Spek, A. L. *PLATON*, Version of August; Program for the Automated Analysis of Molecular Geometry (A Multipurpose Crystallographic Tool); University of Utrecht: The Netherlands, 2006. *J. Appl. Crystallogr.* **2003**, *36*, 7.

(119) De Bruin, T.; Raybaud, P.; Toulhoat, H. *Organometallics* **2008**, *27*, 4864.